Investigating methane cycling conditions & fluxes across a salinity gradient.

James Hensel

Supervisors: Professor Justin Brookes & Dr Christopher Keneally

Submitted in partial fulfilment of the requirements for the degree of Bachelor of Science (Honours), School of Biological Sciences, Department of Ecology and Evolutionary Biology, The University of Adelaide

October 2025

Acknowledgements

I would like to thank everyone who has made this such a wonderful and fulfilling project. Special thanks to my supervisors who have dedicated countless hours to help me develop and learn a new world of skills. To Justin for always providing some clarity and setting my head straight when needed, and to Chris for teaching me, and always pushing me forward. I would also like to give a special thanks to Dr Tony Hall for dedicating his time to help me measure methane and Matilda Southgate for helping my with various calculations.

I am extremely grateful for the opportunities and experiences I've been given through the year by all the people who have come into my world. Particularly Chris, Tyler, Guy, Elyse, Qinqin, Yanhong, Richie, Ava and the other ecologist throughout the Benham. I would also like to thank my beautiful parents Anne and Peter and my housemates Luke, Harry and Michael supporting me through the year.

TABLE OF CONTENTS

1.0 Abstract

Methane cycling within hypersaline systems remains poorly understood, despite its importance in regulating greenhouse gas emissions. Salinity is generally considered a suppressor of methanogenesis by promoting the dominance of competitive sulfate-reducing bacteria (SRB). However, multiple pathways may facilitate methane cycling and atmospheric flux in these environments. To investigate this, we collected sediment cores along a salinity gradient (0-1 g L^{-1}, 15-35 g L^{-1} & > 40 g L^{-1}) and analysed microbial communities (16S rDNA) alongside porewater methane, sulfate and sulfide. Concurrently, methane fluxes were measured using floating chambers equipped with high resolution methane loggers. Our study shows that porewater methane concentrations varied strongly between sites, from 1.5 µM in hypersaline sediments to 3358.7 µM in brackish water. Yet atmospheric fluxes were comparable across all sites with hypersaline sites ranging from 0.68 to 55.11 mg m^{-2} day^{-1} and freshwater from 2.66 to 39.55 mg m^{-2} day^{-1}. PERMANOVA analysis of bacteria and archaeal communities revealed that salinity was the predominant driver in aerobic methane oxidising bacteria (R^2 = 0.306) & anerobic methane oxidising archaea (R^2 = 0.109) community distribution. Further, analysis of methane producers revealed a shift to methylotrophic methanogenesis in hypersalinity. These findings suggest that although methanogenesis is generally suppressed under saline conditions, the combination of shallow production zones and inefficient methane oxidation can still result in significant CH_4 emissions. This highlights that saline environments, often assumed to be negligible CH_4 sources, may be underestimated contributors in global methane budgets.

1.0 Introduction

Increases in atmospheric greenhouse gas (GHG) concentrations are driving higher temperatures, altering rainfall patterns and placing immense pressure on natural systems globally (IPCC 2014). While carbon dioxide (CO_2) is the primary driver of climate change, methane (CH_4) is often overlooked as a significant GHG. However, methane has ~90 times the warming potential of CO_2 on a 30-year timescale making it a shorter acting greenhouse gas and therefore a favourable target for near term mitigation approaches. Methane is strongly influenced by anthropogenic activities, with atmospheric methane concentrations rising approximately 156% during the industrial era (IPCC 2014; Saunois et al. 2020).

Methane originates from natural sources such as wetlands and termites but also from a range of agricultural, fossil-fuel extraction and waste management sources (El-Fadel & Massoud 2001; Johnson & Johnson 1995; Themelis & Ulloa 2007). Methane can be produced biogenically as the final product of decomposition by a group of anaerobic Archaea: methanogens (Saunois et al. 2020; Jackson et al. 2020). In aquatic environments methanogens inhabit waterlogged sediments of wetlands and rice fields where high organic matter content can provide an abundance of substrate to support methanogen communities (El-Fadel & Massoud 2001; Johnson & Johnson 1995) Although most methane emissions are anthropogenic, wetlands contribute 80-280 Tg CH_4 yr^{-1}, representing 20-33% of the global methane budget, or 3.9-16.8 % of total GHG emissions (Bridgham et al. 2013; Saunois et al. 2020). However, “natural” methane sources are often

exacerbated by direct or indirect anthropogenic influence such as in the case of land use change, resulting in higher inputs of nutrients and organic matter.

Coastal ecosystems, which often have higher organic matter inputs than freshwater systems due to integrating larger catchments, are not considered high methane emitters (Hopkinson et al. 1999; Poffenbarger et al. 2011). In sediments, a redox cascade determines the order and depth of oxidants and terminal electron-accepting processes (**Figure 1**). Because sulfate-reducing bacteria (SRB) (SO_4^{2-}) and methanogens exploit common substrates (acetate, H_2, CO_2), they compete for electrons from these organic compounds (Lovley & Klug 1983; Poffenbarger et al. 2011). Therefore, higher coastal sulfur concentrations commonly favour SRB over methanogens, and a negative correlation between CH_4 and salinity is often observed (Poffenbarger et al. 2011). Consequently, coastal systems are generally not considered major methane-producing zones. However, exceptions are increasingly reported, particularly under hypersaline conditions (Chuang et al. 2017; Rosentreter et al. 2018). As such, methane dynamics within coastal systems require further investigation.

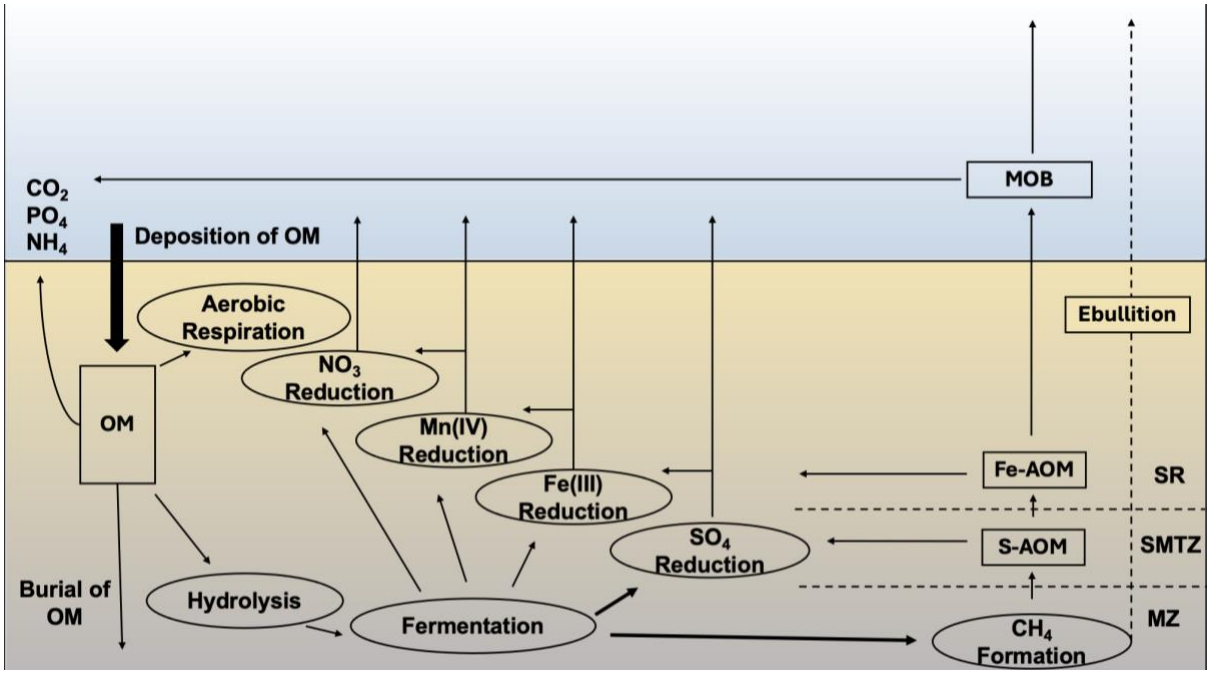

Figure 1: Redox cascade in oxidant use and re-oxidants. As the products of formation are used, methanogenesis and sulfate reduction compete for the final products. After methane is formed it can be re-oxidised through many processes. In the bottom right, MZ is the methanogenic zone, SMTZ is the sulfur-methane transmission zone and SR is the sulfate reduction zone. Adapted from Middelburg and Levin 2019.

Atmospheric methane flux is determined by methane production and consumption. Methane production by methanogenic archaea occurs through three main metabolic pathways: hydrogenotrophic (substrates: H_2/CO_2), acetoclastic (acetate), and methylotrophic (diverse methylated compounds, including methylated thiols and osmolytes such as glycine betaine) (Wallenius et al. 2021). Most biogenic methane is produced via hydrogenotrophic and acetoclastic pathways in low-sulfate environments, whereas methylotrophic methanogenesis is often more common in saline systems due to less competition for substrates (Lovley & Klug 1983; Keneally et al. 2024). Methane consumption can occur aerobically, mediated by methane-oxidising bacteria (MOB), or

anaerobically, predominantly through the sulfur-dependent anaerobic oxidation of methane (S-AOM) among other pathways (N-AOM & Fe-AOM) performed by anerobic methanotrophic archaea (ANME) (Wallenius et al 2021). AOM occurs in a specific zone in sediments called the sulfur-methane transition zone (SMTZ) in which as sulfate concentrations deplete, methane concentrations increase, allowing for ANME to access both substrates (**figure 1**). Factors such as increased organic matter loading can favour methane production, while aerobic MOB are limited by oxygen availability (Myllykangas et al. 2020 & Schorn et al. 2024). ANME are further susceptible to shifting redox conditions and sulfide (H_2S) toxicity (Dalcin Martins et al. 2024). High organic matter and reducing redox conditions are characteristic of methane emitting systems but have not been fully explored in coastal environments. While the rates of production and consumption of methane are the key constituents that dictate atmospheric flux rates, physical parameters can also result in significant variability. Methane solubility in water is affected by temperature, salinity and pressure (Wiesenburg & Guinasso 1979). Changes in these physical parameters can therefore influence the method and rate that gas can escape a fluid (being diffusion (movement of gas) and ebullition (bubble formation)) (Wiesenburg & Guinasso 1979).

Eutrophication, or excessive nutrient input, can greatly disrupt the balance between microbial methane production and consumption (Beaulieu et al. 2019). In coastal systems, two main drivers of eutrophication are elevated nutrient inputs and reduced flows (Bricker et al. 1999; Chilton et al. 2021; Swaney et al. 2008; Steward & Lowe 2010; Le Moal et al. 2019). Both of these drivers promote organic matter accumulation, which can result in depositional zones of toxic monosulfidic black oozes (MBOs)(Mosley et al.

2020). These depositional zones have been found to drive methane production within saline systems (Keneally et al. 2024), but the governing mechanisms remain poorly understood. With eutrophication and salinisation likely to increase in the future (Jeppesen et al. 2020; et al. 2019; Keneally et al. 2025b), it is vital to develop a mechanistic understanding of methane dynamics within coastal systems to inform management strategies.

The Coorong is a coastal lagoon wetland system in South Australia, recognised as internationally important under the Ramsar Convention as acritical habitat for migratory wader birds (Mosley et al. 2018). Located at the terminus of the Murray-Darling Basin, the ecosystem has become extremely hypersaline and hypereutrophic (total nitrogen, TN > 4 mg L^{-1}; total phosphorus, TP > 0.2 mg L^{-1}; chlorophyll a > 50 μg L^{-1}) due to reduced freshwater inflows and increased evapoconcentration (Mosley et al. 2023). Initial surveys have indicated positive correlations between salinity and both porewater, and surface water methane concentrations under hypersaline conditions (Keneally et al. 2024). Similarly, methylotrophic methanogenesis pathways are likely dominant in the Coorong, indicating the potential for non-competitive substrate-based methanogenesis (Keneally et al. 2025). However, a holistic understanding of methane generation and consumption in the Coorong, incorporating fluxes, pools, and microbial communities, remains elusive, despite the advantage of studying such dynamics across the wide range of salinities within the a single system.

In this thesis, methane cycling along the Coorong's salinity gradient, including both sedimentary production and areal fluxes to the atmosphere was investigated. Four sites

were selected based on salinity (hypersaline [>40 g L^{-1}], brackish [5-30 g L^{-1}], and fresh [<1 g L^{-1}]) and sediment conditions. Sediment cores were collected and sectioned at four intervals from each site to assess sediment chemistry, prokaryotic microbial communities, and benthic methane flux rates, alongside atmospheric methane flux and methane water column concentrations. This thesis aims to.

1) Quantify methane flux rates within the Coorong and across a salinity gradient.
2) Investigate the influence of salinity on methanogenic and methanotrophic microbial communities.
3) Identify the key differences in potential methane flux pathways across a salinity gradient through investigating chemical, physical and biological components.

2.0 Methods

3.1 Site description and sampling techniques

The Coorong is a shallow coastal lagoon within South Australia, connected to the Southern Ocean through the Murray Mouth, at the estuary of the Murray-Darling Basin. The lagoon is divided into the North and South lagoons by a constriction at Parnka Point (**Figure 1**). Freshwater flows to the Coorong mainly come from the Murray River, though the lower lakes (Lake Alexandrina and Lake Albert) and exit out through the Murray Mouth. At the mouth, mixing with seawater from the Southern Ocean occurs. Due to net evaporation, the Coorong becomes increasingly saline and sulfate rich further south along the lagoons, away from major inflows (**Figure 1**).

Samples were taken from a total of 4 sites, with 2 being in the South lagoon, 1 within the north lagoon and 1 within Lake Albert, acting as a freshwater "methane favoured" control site (**Figure 2**). Water column parameters were measured at each site using a calibrated multiparameter sonde: YSI Exo 2 (Yellow Springs Instruments, Ohio, USA). To assess the sediment microbial community, sediment cores were taken with a custom ball valve-sampler using screw-fitted acrylic cores (60 mm internal diameter [I.D.]), in triplicate at each site. Prior to sampling, cores were sterilised in 10% v v^{-1} bleach solution. The upper 15cm of sediment cores were sliced at ~3-4 cm intervals and each slice homogenized on a portable, sterilised bench. Homogenised sediment subsamples (3 mL) were then preserved within LifeGuard solution (Qiagen, Hilden, Germany), in sterile DNAse/RNAse free 15mL tubes, and frozen at -20°C within 1h of sampling. To account for potential contamination, additional "field blank" samples of the processing station and utensils

were collected from each site. 'Field blank' samples were then used to remove potential contaminants from the sequencing dataset *in silico*.

A further six sediment cores were collected per site, with bleach pre-sterilised PVC tubes (50 mm I.D.) for 1) porewater methane and SO_4^{2-} concentrations (3 cores) and 2) DGT sulfide probes (3 cores). To sample porewater methane, 2 cm^3 sediment samples were taken from depths ranges of 2-4cm, 6-8 cm, 10-12 cm, and 14-16 cm through pre-drilled holes which are taped during coring. Sediment was quickly extruded with a sterile, cut-off 20 mL syringe, without introducing air bubbles, into a 12 mL evacuated exetainer (Labco, UK) containing 1 mL of 8 M potassium hydroxide solution, to immediately halt bacterial activity. Exetainers were quickly sealed with caps and stored at 4°C until analysis. For SO_4^{2-}, bulk sediment was taken at 4 depth ranges (as described above), then transferred to sterile DNAse/RNAse free 15mL tubes and frozen at -20°C within 1h of sampling. Porewater was later extracted by centrifuging thawed sediment at 5000 × *g* for 15 min in a 50 mL centrifuge tube. Representative water samples for water column methane were collected *in situ* from 50 cm below the water surface using a 140 mL syringe. To facilitate gas headspace equilibration, 35 mL of water was expelled, replaced with ambient air, shaken, and then 20 mL of the headspace gas is injected into a 12 mL evacuated exetainer (Labco, UK).

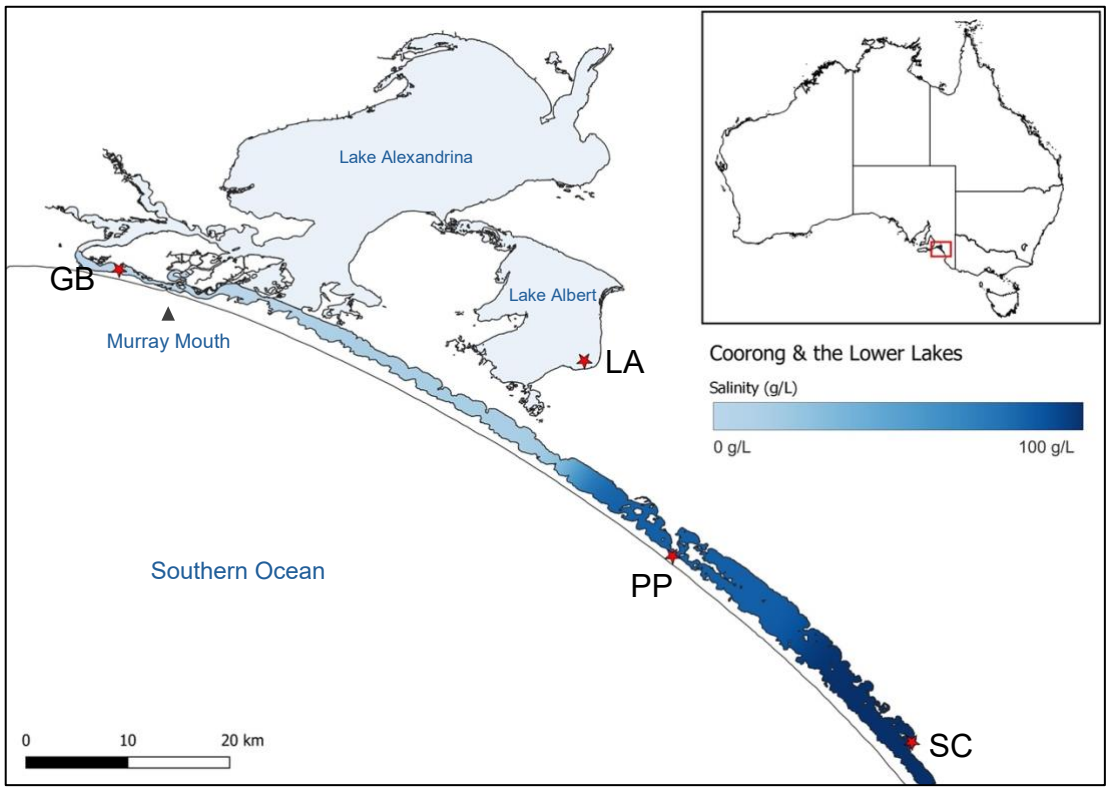

Figure 2. Map of the study location with sampling sites marked. Sampling sites are Lake Albert (LA), Goolwa Barrage (GB), Parnka Point (PP) and Salt Creek (SC).

3.2 Methane flux chamber deployment and calculations

A key component of this study was to measure atmospheric methane flux, given its significance to the cycling processes occurring within the sediments. To do this, methane flux chambers were assembled as per Sø et al. (2024), using an Arduino-based logger to automatically record atmospheric methane, relative humidity, and temperature, at high resolution (0.5 hertz). Sensors were calibrated previously described by So et al (2024), using a Picarro G2201-i Isotopic Analyzer cavity ring down spectrometer (CRDS) (Picarro, CA, USA), with a methane gas standard of known concentration (700ppm; BOC, UK) that was introduced to the sensors and allowed to dissipate over time. Sensors were

mounted inside the top of floating 20L upside-down buckets, inside 500mL plastic Sistema KlipLock containers, ensuring that they avoid contact with salt without influencing chamber gas circulation. Flux chambers were deployed in a minimum of triplicate at each site under minimal wind conditions, attached in by ropes to float in series downstream of an anchored buoy. Due to sensor complications, no data was recorded during the initial sampling trip. Sampling resumed on later trips during, Winter (10th to 12th July) and Spring (22nd to 26th September), allowing for seasonal variance analysis. To further constrain sensor calibrations under field conditions, gas samples were taken *in situ* through a sample port in the chamber, as described by Bastviken et al. (2020). Gas samples were then measured using a GC-FID (**See section 3.4**). After deployment for greater than 1 h, high resolution sensor data running variance was processed and interpreted based on the methods outlined in Sø et al. (2023), to estimate both diffusive and ebullitive fluxes.

3.3 Deployment, retrieval and processing of sulfide DGTs

To understand the potential influence of sulfide inhibition on methanotrophic taxa, dissolved sulfide concentrations were determined with diffusive gradients in thin films (DGTs). DGTs passively accumulate dissolved substances on binding layers giving an *in situ* representation of analyte concentrations. Sediment cores for DGT probes were taken so that the sediment surface was within 5cm of the core rim, topped with site water, and capped for transport. For deployment, methods were followed as per Huang et al. (2025) with slight modifications. Cores were transported to accommodation close to field sites for processing, where incubations were conducted in triplicate over a 5 h or 24 h period depending on expected concentration. Buckets filled with site water were used as small

scale mesocosms while being aerated with an aquarium pump to maintain water column oxygenation, and to circulate water over the top of cores (**See Appendix G**).

The DGT probes were deployed by gently inserting them into the central part of cores or inserted with the aid of a flat object such as a ruler in the case of coarse sediments. Probes were inserted so that the sedimentary interface was roughly 13 - 15 cm along the probe.

Following the deployment periods, the DGT probes were carefully retrieved from the sediment and immediately rinsed with deionised water to remove any attached sediments. The probes were then be stored in individual polyethene bags with deionised water to avoid dehydration until analysis. For analysis, probes were dismantled and scanned following the procedures described by Robertson, Teasdale and Welsh (2008).

3.4 Methane and sulfate sampling and concentration calculations

Both water column, and porewater measurements of methane can provide insights to understanding the cycling processes occurring at each site (Krause et al. 2023). Additionally, sulfate concentrations are needed to understand potential competition for substrates. For water column methane concentrations, 500 µL of sample headspace was injected into an Agilent 7890B GC-FID (Agilent, CA, USA) equipped with a PoraBOND U 25 m x 0.32mm x 7 µm column (Agilent, CA, USA) heated to 100 °C with hydrogen as a carrier gas. Peak areas were derived from produced chromatographs and concentrations were subsequently calculated according to Johnson et al. (1990) & Magen et al. (2014). For porewater samples, headspace equilibration was performed on samples in stored exetainers within 4 weeks of sampling. Immediately after equilibration samples were processed the same as water column samples. To account for variation in sample water

content, porewater volumes were determined gravimetrically, with each sample being weighed before, and porewater content being calculated based of sediment water content. Porewater SO_4^{2-} samples were analysed after centrifuge extraction through the turbidimetric standard method of Baird et al. (2017) (4500-SO42-E) (detection limit: 1-40 mg L^{-1}). Due to high concentrations, porewater was diluted with reagent water by a factor of 200 (0.5mL per 100mL) for hypersaline sites, 20 (5mL per 100mL) for freshwater sites, and 100 (1mL per 100mL) for estuarine sites.

3.5 Organic Matter and Soil Physical Properties

To approximate the indirect proportion of carbon at each site, total organic matter content was determined gravimetrically using the loss on ignition (LOI) method (Heiri, Lotter & Lemcke 2001). Sediment aliquots (0.5-2g) were taken from four depths (3 cm, 7 cm, 11 cm, and 15 cm) in each core. The aliquots (n = 5) were dried at 60°C for several days to remove water from the samples. The sediment water content was then determined when the final weight lost from each sample had plateaued (maximum 4% weight lost per day). The samples were then heated at 400-500°C in a muffle furnace for one hour and reweighed for the determination of organic matter content (% per g dry weight).

3.6 DNA Extractions, Amplicon sequencing and Bioinformatic Processing

To extract DNA, the Qiagen PowerSoil Kit (Qiagen, Hilden, Germany) was used following kit instructions. Each sample was subsampled and extracted in duplicate to account for potential technical variation. Extract concentrations were measured using a Qubit (Thermo Fisher Scientific, USA). For amplification two approaches were used. To understand Bacterial community composition, the 16S (V1-V3) rDNA gene was amplified, followed by paired-end sequencing performed by the Australian Genome Research Facility (AGRF, Queensland). Amplification was performed using: 16S-27_F (forward) 5′-AGAGTTTGATCCTGGCTCAG-3′ and 16S-519_R (reverse) 5′-GWATTACCGCGGCKGCTG -3′ primers. Additionally, the Archaeal community was assessed by amplification of the 16S (V3-V4) rDNA gene, followed by paired-end sequencing performed by Biomarker Technologies (BMKGENE, Hong Kong). A nested PCR design was used, with the first stage using: GU1ST-340F (forward) 5'-CCCTAYGGGGYGCASCAG-3' and GU1ST-1000R (reverse) 5' GAGARGWRGTGCATGGCC-3' primers, and the second stage using: Arch349F (forward) 5′-GYGCASCAGKCGMGAAW-3′ and Arch806R (reverse) 5′-GGACTACVSGGGTATCTAAT-3′ primers. For each amplicon, the samples were demultiplexed and denoised using DADA2 in Quantitative Insights Into Microbial Ecology (QIIME) 2 software. The resulting Amplicon Sequence Variants (ASVs) were assigned taxonomy with a 16S V3-V4 classifier trained on Silva v138.2 99% reference sequences. Field and technical blanks were accounted for using the R package *Decontam* (Davis et al. 2018).

3.7 Methane Diffusion Calculations

Sediment Diffusion Calculations

Sediment to water methane flux was calculated by Fick's first law of diffusion:

$$J = -\phi D_s \cdot \frac{dC}{dz} \quad \textbf{Eq. 1}$$

Where J is the diffusive flux (mmol m^{-2} d^{-1}), ϕ represents the sediment porosity, $D_s$represents the sediment diffusion coefficient for the *in-situ* tortuosity, pressure, temperature and salinity (calculated in the R package *marelac* (Soetaert et al. 2010)), and $\frac{dC}{dz}$ is the methane concentration gradient from the top 3 cm of sediment into the water column. Sediment porosity was calculated from the following two relationships outlined in Håkanson and Jansson (2002):

$$P_b = \frac{100 \cdot P_m}{100 + (WC + OC)(P_m - 1)} \quad \textbf{Eq. 2}$$

Where $P_b$represents bulk density, P_m represents the density of inorganic particles (taken as 2.6 g cm^{-3}), WC is the water content and OC is the organic matter content. Sediment porosity can then be estimated as:

$$\phi = 1 - \frac{P_b}{P_m} \quad \textbf{Eq. 3}$$

3.8 Statistical Analysis

Statistical analysis was conducted using R (v4.4.1) (R Core Team, 2024) and MATLAB (v24.2.0.2863752). Permutational multivariate ANOVA (PERMAONVA) and beta-dispersion testing were conducted to analyse community β-diversity using *vegan* (Oksanen et al. 2025). Kruskal-Wallis *H* tests and Dunn's test with *p* value adjustment for the false discovery rate (*post hoc*) were implemented to test significant difference between community α-diversity and methane porewater concentrations and flux rates.

Basic relationships between environmental variables were tested with Spearman's rank-order correlation. Gas coefficients were derived and calculated with *marelac* (Soetaert et al. 2010).

Methanogenic and methanotrophic taxa were identified through the use of the Functional Annotation of Prokaryotic Taxa (FAPROTAX) database (Louca et al. 2016). FAPROTAX maps prokaryotic clades to establish metabolic or ecologically relevant functions using the current literature on cultured strains (Louca et al. 2016). Due to the conservatism of the FAPROTAX approach (e.g. reliance on cultured strains of notoriously difficult-to-culture Archaea from extreme environments) (Solden et al. 2016), slight modifications were applied to broaden the scope of the database. These mainly included using family level classifications as well as some manual adjustments to the database such as including various ANME classifications where no cultured strains exist, but the function is well supported by genomic approaches in the literature. A table of revisions made to the FAPROTAX database and output is provided in appendix D.

3.0 Results

4.1 Site characteristics

Salinity increased progressively away from the Murray Mouth, reaching extreme hypersaline levels at the southern sites (**Table 1**). Sampling sites were generally shallow and well-mixed, except for GB, which exhibited salinity stratification likely due to frequent freshwater inflows from the nearby barrage (**Figure S1**). Water column CH_4 concentrations varied between sites, with the highest recorded at GB (0.55 µM) and the lowest at SC (0.03 µM).

Table 1: Mean water column parameters measured *in situ*. Data was derived from initial Autumn sampling trip.

Site	**Water Depth (m)**	**WC Temperature (°C)**	**WC Salinity**	**WC CH_4 (µM)**	**WC pH**	**Salinity Category**
Lake Albert (LA)	1.3	18.21	0.63	0.27 ± 0.189	8.92	Freshwater
Goolwa Barrage (GB)	1.1	20.87	23.61	0.55 ± 0.029	7.96	Brackish
Parnka Point (PP)	0.5	19.93	86.28	0.14 ± 0.014	8.27	Hypersaline
Salt Creek (SC)	0.6	19.76	97.27	0.03 ± 0.004	7.78	Hypersaline

4.1.3 Atmospheric methane fluxes

Despite large differences in porewater CH_4 pools (**Figure 3A**), sediment-to-water (S-W) column fluxes (from the top 3 cm to the water column) were similar between freshwater and hypersaline sites (**Figure 3B**). GB exhibited significantly higher S-W fluxes (H: 10.54 $p < 0.01$; **Figure 3B**), likely reflecting its elevated water column CH_4 concentrations and surface sediment production. In July, there was no significant difference between

atmospheric flux rates, while September sampling showed a weakly significant decrease at hypersaline sites when compared to fresh and brackish (H: 9.19; p <0.05; Figure **3C**). Atmospheric flux rates were likely lower in September due to cold water temperatures moving out of Winter. There was no recorded ebullition during sampling although potential methane bubbles were observed in surrounding waters.

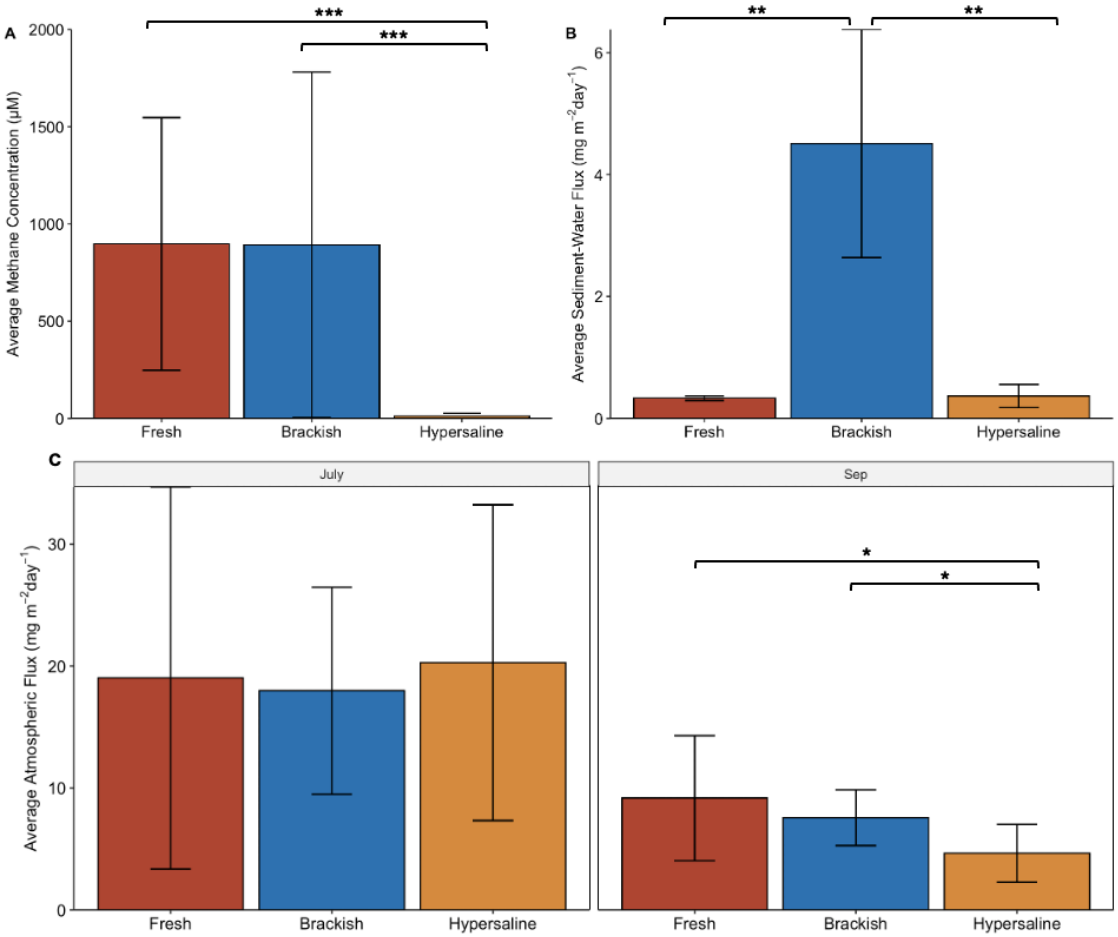

Figure 3: Methane concentration across sediment to atmosphere continuum where A) Average methane concentration in porewater; B) Average sediment-water methane flux rate; C) Average atmospheric methane flux rate from July & September. Large standard deviation for A) are due to concentrations being averaged from shallow to deep samples. No data was recorded at SC for atmospheric flux rates in September. Results from Kruskal-Wallis *H* tests are displayed on the figures with Dunn's test with *p* value adjustment for the false discovery rate (***$p < 0.001$; **$p < 0.01$; *$p < 0.05$).

4.1.2 Porewater chemistry

OM content was relatively consistent with increasing depth at LA and GB, though slightly higher at GB (**LA & GB; Figure 3**). In contrast, hypersaline sites displayed clear trends of organic matter deposition in surface sediments followed by rapid carbon depletion with depth. PP recorded the highest organic matter content (10-15%) in the 0-7 cm range, decreasing to 4% by 11 cm depth. Porewater methane showed no clear relationship with organic matter at LA and GB, as concentrations gradually increased with depth. Notably, methane production at GB appeared to occur much closer to the surface than at LA, reaching ~500 μM by 3 cm depth compared to ~59 μM at LA (**LA & GB; Figure 3**). Methane concentrations in these two lower salinity sites either reached (**LA; Figure 3**) or approached local saturation at depth (**GB; Figure 3**), suggesting the potential for bubble formation within sediments. Hypersaline sites contrasted sharply with fresher sites, showing the highest methane concentrations in surface sediments that decreased with both depth and organic matter content. Overall, porewater CH_4 concentrations were lower at hypersaline sites.

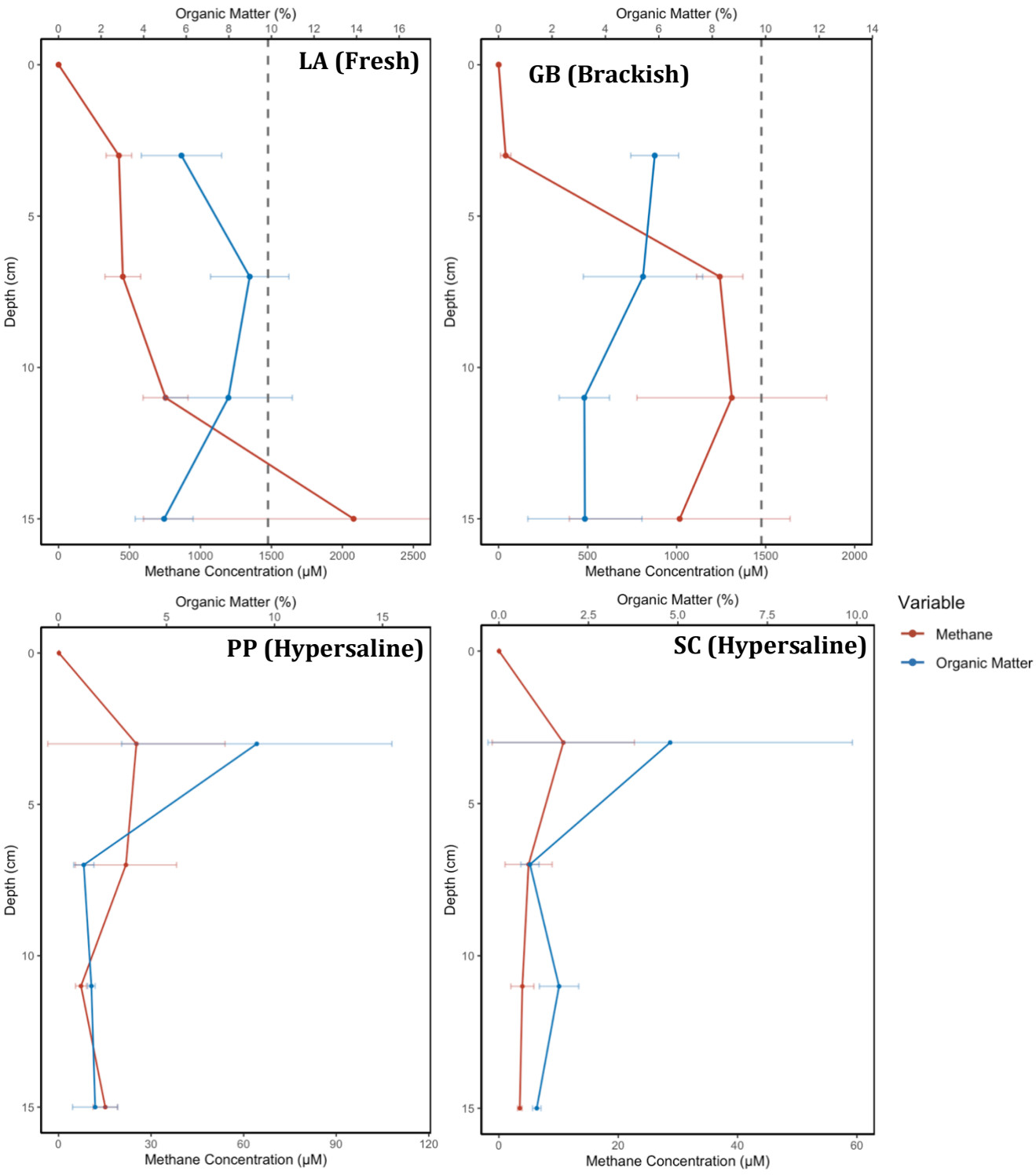

Figure 4: Porewater methane and organic matter concentration profiles through first 15 cm of sediment of LA) Lake Albert (LA); GB) Goolwa Barrage; PP) Parnka Point; SC) Salt Creek. Organic matter is calculated as % of organic matter g^{-1} dry soil. Vertical dotted lines are methane porewater saturation concentrations assuming methane has a pure gas phase. Water column data for methane is plotted at 0 cm depth.

Suggested locations of the SMTZ are displayed with grey. Note changing scales of X axis across figure.

Sulfate concentrations were enriched in hypersaline sediments, being up to 2-3 times the concentration of seawater (seawater: ~2.65 g L^{-1} SO_4^{2-}). Sulfate was lowest at LA (<0.1 g/L) and highest at SC (>5 g/L) (**LA & SC; Figures 4**). Sulfate displayed no clear depth-related trends, aside from at GB, where a gradual decrease was observed (**GB; Figure 4**). CH_4 production appeared suppressed under extremely high sulfate concentrations but remained substantial under moderate levels (~1 g/L), as observed at GB (**PP & SC; Figures 4**). Sulfide was also prevalent under high salinity, rapidly accumulating close to the sediment surface (**PP & SC; Figures 4**). Interestingly, despite lower sulfate concentrations at GB compared to hypersaline sites, dissolved sulfide reached comparable levels (~300 μM) (**GB; Figure 4**).

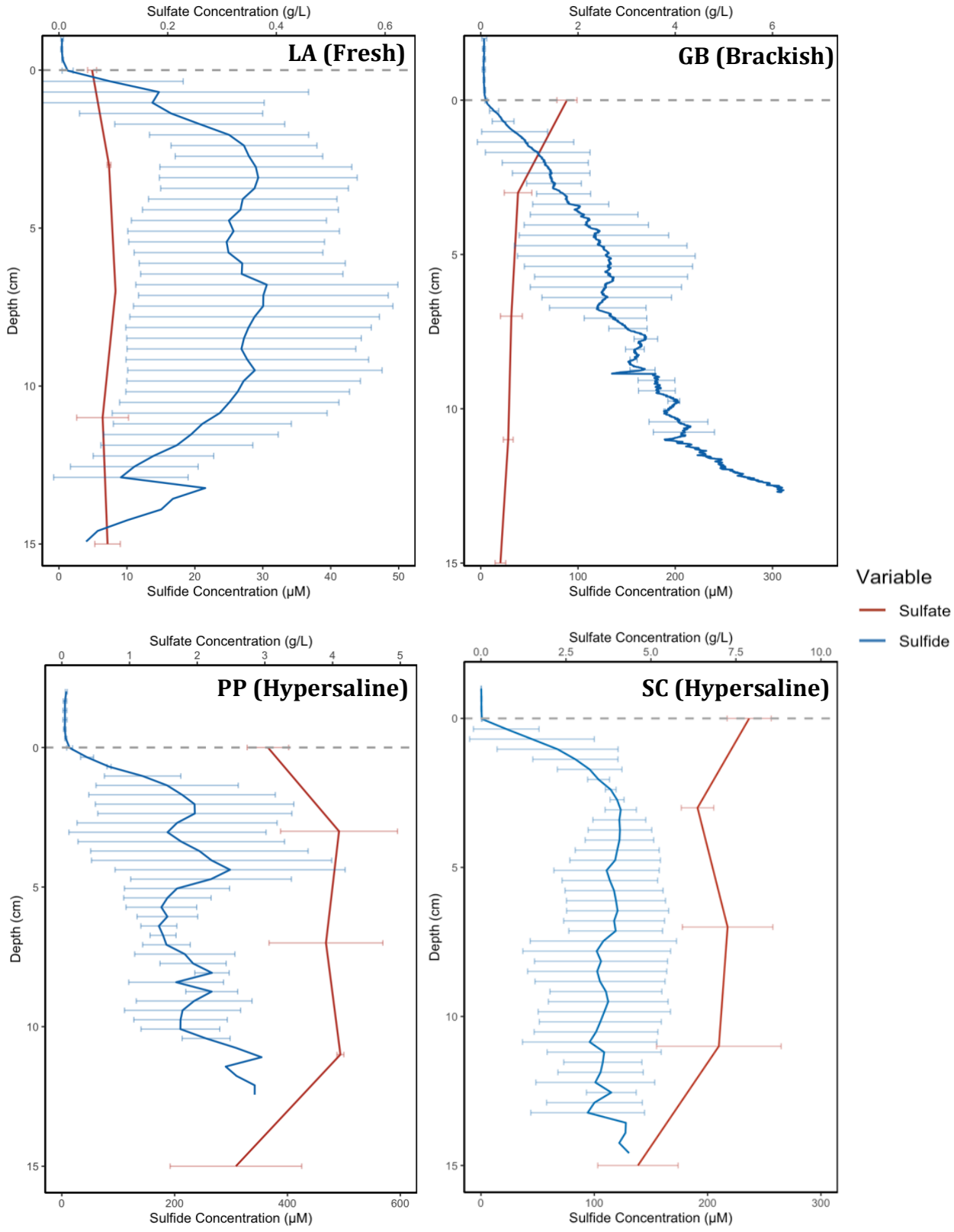

Figure 5: Porewater Sulfide and Sulfate concentration profiles through first 15 cm of sediment of LA) Lake Albert (LA); GB) Goolwa Barrage; PP) Parnka Point; SC) Salt

Creek. The water-sediment interchange is indicated by the grey dashed line. High resolution 1D sulfide data was binned by depth for visualisation. Note changing scales of X axis across figure.

4.2 Microbial ecology

4.2.1 Whole community β-diversity

Bacterial and Archaeal community β-diversity analyses revealed significant shifts along the salinity gradient. In bacterial communities, clustering occurred primarily by salinity group, with fresher sites being associated with higher porewater CH_4 and organic matter (**Figure 6A**). Hypersaline sites were more associated with sediment bulk density, sulfate, and sulfide. Freshwater sites also showed depth-based separation, particularly among shallow sediments likely dominated by photoautotrophic bacteria. Salinity emerged as the primary driver of β-diversity (R^2 = 0.173, p <0.01), followed by smaller contributions from sulfate (R^2 = 0.069, p <0.01) and organic matter content (R^2 = 0.039, p <0.01).

Archaeal community β-diversity patterns largely mirrored those of bacterial communities, with clear salinity-driven groupings (**Figure 6B**). Fresh and brackish samples formed tighter clusters, associated mainly with porewater CH_4, while hypersaline samples displayed more dispersed communities (driven by the broad salinity range) linked to salinity, bulk density, sulfate, and sulfide. Organic matter content was most strongly associated with brackish communities. Depth-related trends were most evident in freshwater sites, with some clustering among brackish samples (**Figure 6B**).

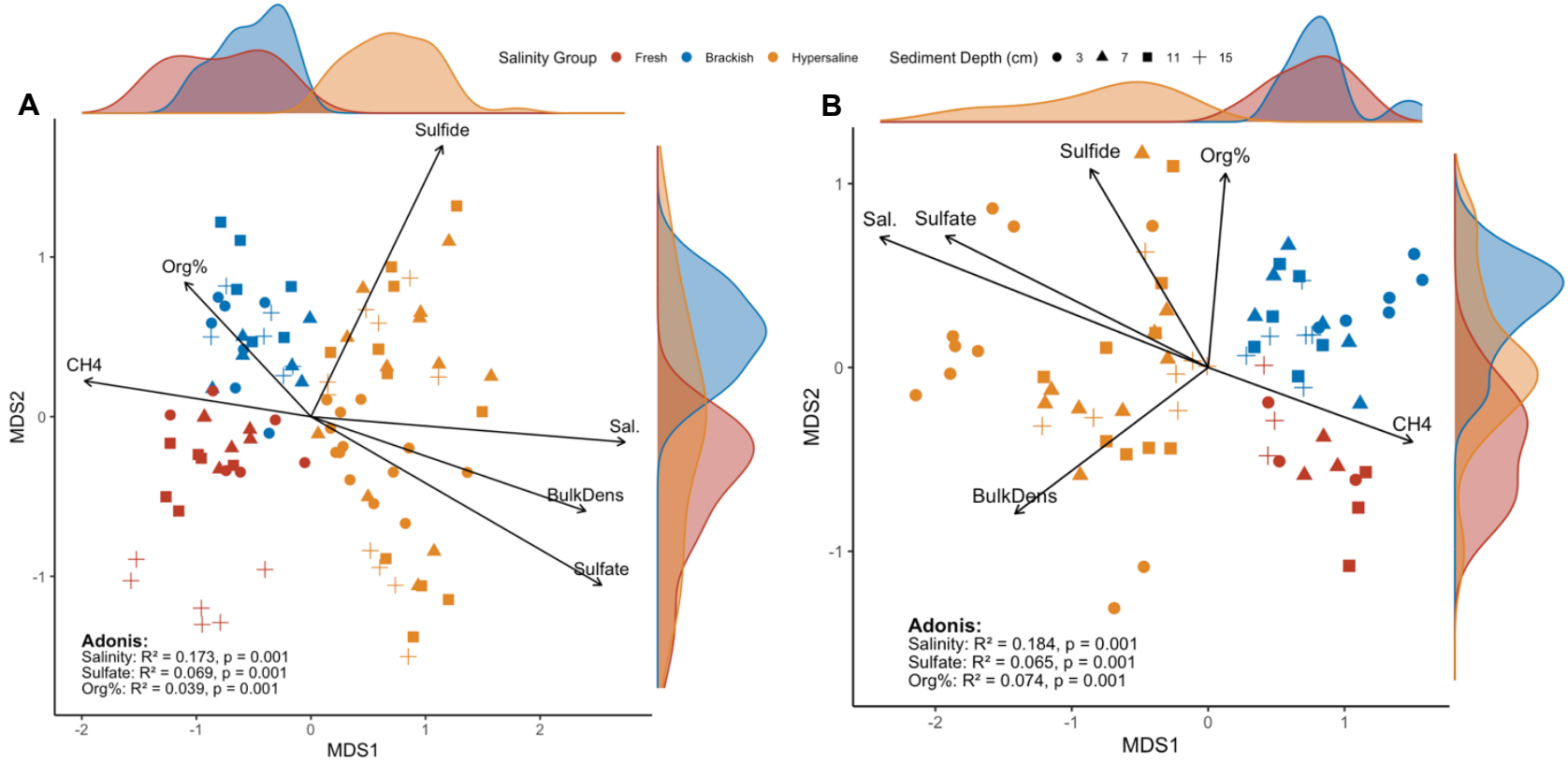

Figure 6: Microbial community β-diversity. Visualised using MDS, with Euclidean distances where A) Bacteria community; B) Archaeal communities. Relevant environmental variables are fit to the ordination, with strength of relationships represented by arrow length. Results of significant PERMANOVA (Adonis) test are displayed, indicating a separation between the centroids of the two groups. Beta dispersion values for **A)** F-value: 9.3236. *p*-value: 0.000204. and for **B)** F-value: 16.913. *p*-value: 1.092×10^{-6}.

4.2.2 Methane cycling community α-diversity

Methane-cycling communities including methanogens, methane-oxidizing bacteria (MOB), and anaerobic methane oxidizers (ANME) showed significant variation in α-diversity along the salinity gradient. There was a marked decline in methanogens as salinity increased (**Figure 7A**), while Shannon diversity remained similar between fresh and brackish samples. MOB displayed a contrasting pattern, with hypersaline samples showing substantially lower diversity across both metrics (**Figure7B**). ANME followed a similar trend, being virtually absent from hypersaline sediments (**Figure 7C).**

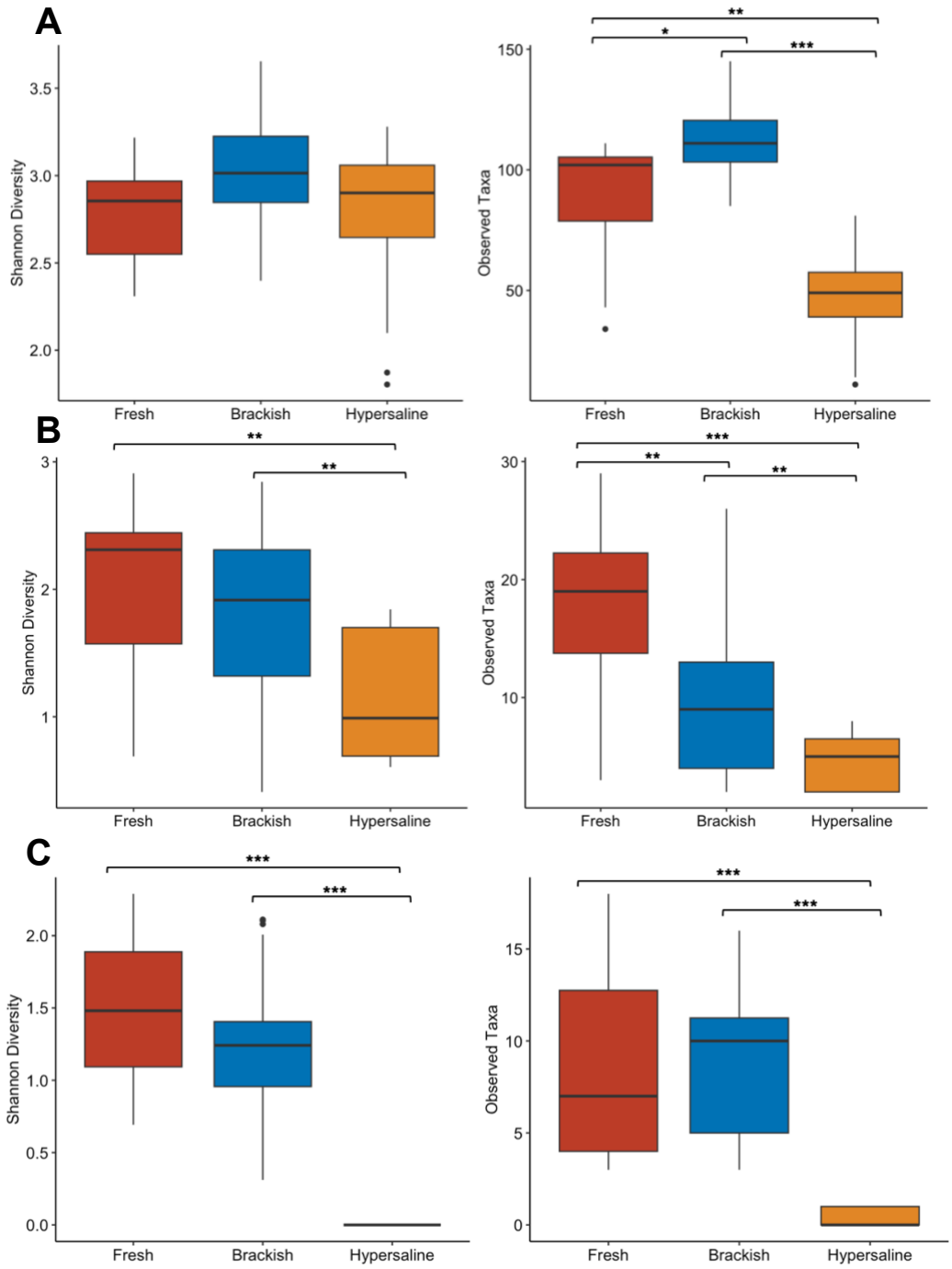

Figure 7: Alpha Diversity of A) Methanogens; B) MOB; C) ANME across salinity categories visualised as Shannon diversity and observed taxa. Kruskal-Wallis *H* tests are displayed on the figures with Dunn's test with *p* value adjustment for the false discovery rate (***$p < 0.001$; **$p < 0.01$; *$p < 0.05$). Note changing scales of Y axis.

4.2.3 Methane Cycling Community β-diversity

Methanogenic community β-diversity revealed distinct groupings along the salinity gradient (**Figure 8**). Similar to whole-community β-diversity, hypersaline samples were more strongly associated with salinity and sulfate, whereas brackish samples aligned more closely with organic matter content and porewater methane. PERMANOVA (Adonis) analysis confirmed that salinity was the primary driver of methanogenic β-diversity ($R^2 = 0.294$).

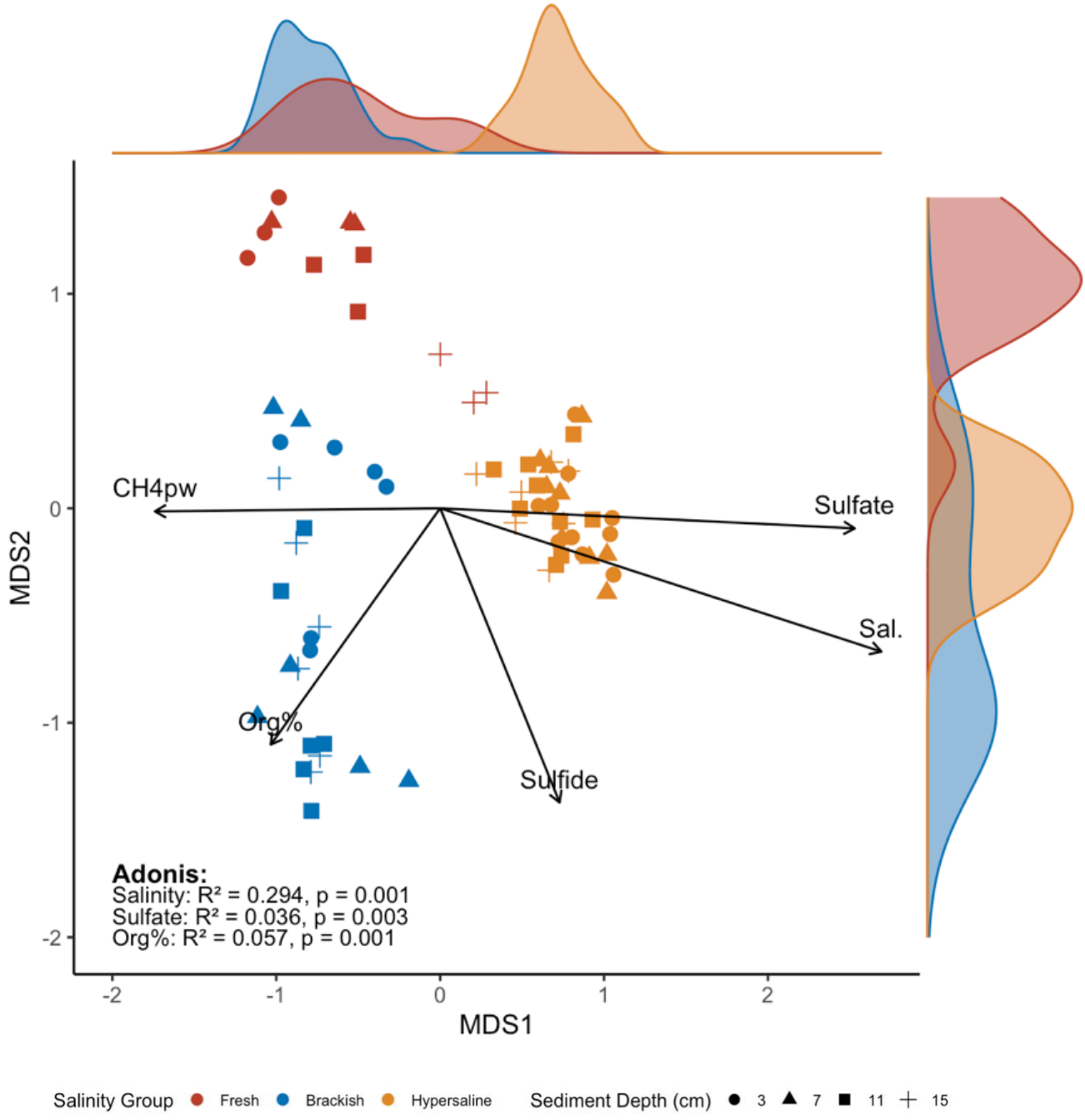

Figure 8: Methanogenic community β-diversity visualised using MDS, with Euclidean distances. Relevant environmental variables are fit to the ordination, with strength of relationships represented by arrow length. Results of significant PERMANOVA (Adonis) test are displayed, indicating a separation between the centroids of the two groups. Beta dispersion values are F-value: 5.5966. *p*-value: 0.00562.

Continuous variables were also tested for their influence on MOB and ANME β-diversity using PERMANOVA (**Tables 2 & 3**). In both cases, salinity emerged as the dominant factor (*Adonis:* R^2 = 0.306 for MOB; R^2 = 0.109 for ANME; *p <0.001*). Organic matter content also had a significant influence on both taxonomic groups (*Adonis:* R^2 = 0. 02302 for MOB; R^2 = 0.07458 for ANME; *p = 0.003*). Porewater methane and sulfide were additionally significant predictors within ANME communities (**Table 3**), but not within MOB. It is key to note that the group dispersion between fresh, brackish and hypersaline categories is uneven on each analysis (Beta Dispersion: $p < 0.05$). In cases where a design is unbalanced (like this example), and the larger group has greater dispersion, PERMANOVA test can be considered conservative (Anderson & Walsh, 2013). Although, often due to target species being rare within samples (ANME/MOB), and the larger group being a hasher environment (hypersaline), larger groups tend to exhibit smaller dispersion. In cases such as this PERMANOVA test can be too liberal, meaning results presented should be interpreted with care (Anderson & Walsh, 2013).

Table 2: Effect of continuous variables on MOB community β-Diversity. PERMANOVA (Adonis) and permutational β-Dispersion analysis results for hypothesis testing on continuous variables associated with MOB community β-Diversity, expressed as Euclidean distances.

		Adonis			***Beta Dispersion***	
Factor	**Df**	**F-value**	**R2**	**p-value**	**F-value**	**p-value**
Salinity	1	10.8942	**0.30693**	**0.001**		
Porewater CH4	1	2.0536	0.01198	0.105		
Sulfate	1	0.8253	**0.03286**	**0.002**		
Org%.	1	1.7557	**0.02302**	**0.003**		
Sulfide	1	1.6096	0.00908	0.177		
Residuals	88		0.79741	0.196		

Total	95	1.000	**5.933**	**0.0009575**

Table 3: Effect of continuous variables on ANME community β-Diversity. PERMANOVA (Adonis) and permutational β-Dispersion analysis results for hypothesis testing on continuous variables associated with ANME community β-Diversity, expressed as Euclidean distances.

	Adonis				**Beta Dispersion**	
Factor	**Df**	**F-value**	**R2**	***p*-value**	**F-value**	***p*-value**
Salinity	1	10.3857	**0.10913**	**0.001**		
Porewater CH4	1	5.8469	**0.06144**	**0.002**		
Sulfate	1	2.5742	0.02705	0.052		
Org%.	1	7.0982	**0.07458**	**0.003**		
Sulfide	1	4.2652	**0.04482**	**0.013**		
Residuals	65		0.68299	0.196		
Total	75		1.000		59.949	$\mathbf{9.81 \times 10^{-16}}$

4.2.4 Methanogenic pathway identification

Methanogenic taxa identified through FAPROTAX indicated that hydorgenotrophic utilising taxa were most abudant at brackish and fresh sites, whereas methylotrophic utilising taxa were most abudant at hypersaline sites (**figure 9**). Taxa using acetoclastic pathways were absent from hypersaline sites, and second most abudant at brackish sites. Flexible metabolism was most abudant at fresh, where soley methyltrophic taxa were absent.

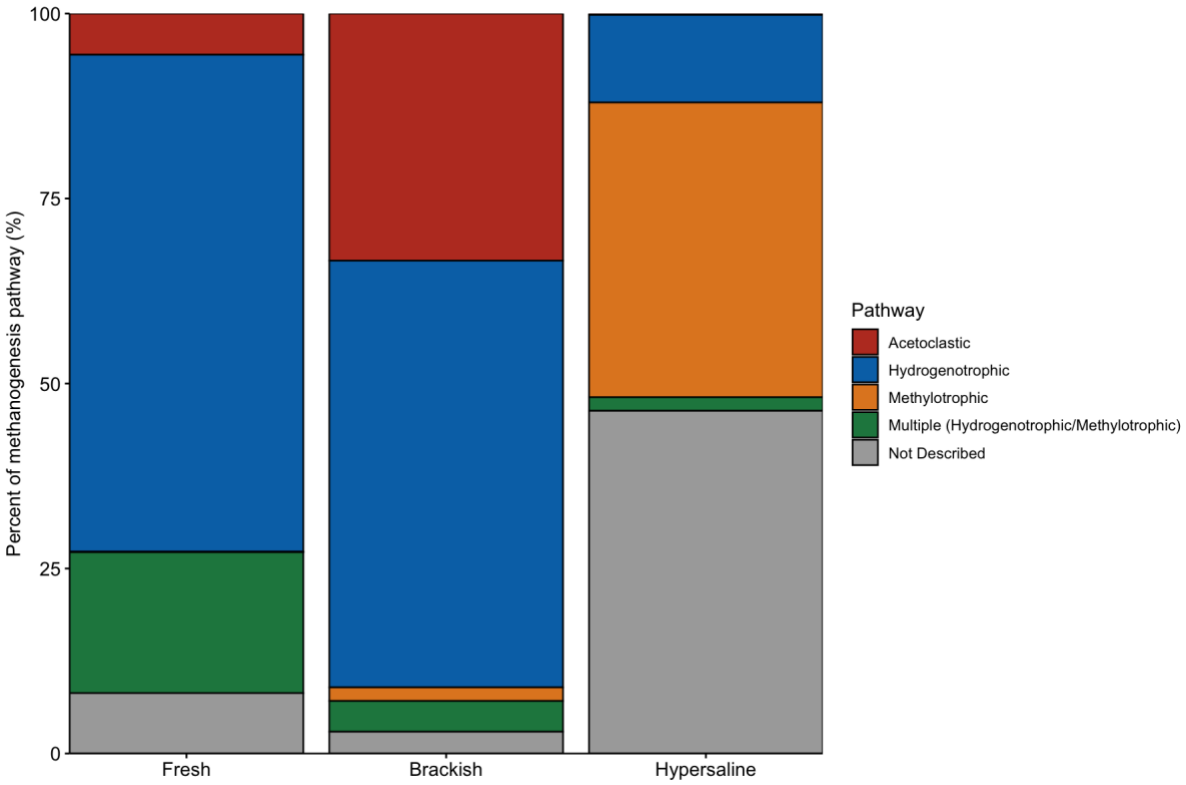

Figure 9: Proportion of methanogenesis pathways occurring at each salinity group. Methanogenesis pathways were identified based on the relative proportion of methanogenic OTUs associated with each pathway as determined by FAPROTAX.

4.0 Discussion

While previous studies have highlighted the potential for methane generation within the hypereutrophic hypersaline Coorong (Keneally et al. 2024, Keneally et al. 2025), none have provided evidence of atmospheric fluxes. This study describes how microbial communities and physical and chemical parameters result in changing methane flux rates across salinity gradients. This provides a mechanistic understanding to support our knowledge on eutrophication-driven organic matter accumulation and methane production "hotspots" in surface sediments (Keneally et al. 2024).

This study suggests that even though sulfate is not limited within the Coorong, methane production can still occur at sufficiently high rates to drive substantial atmospheric emissions. Methane production in hypersalinity can be facilitated by a shift to methylotrophic pathways which is supported thoroughly through the literature (Keneally et al. 2024; Keneally et al. 2025; Krause et al. 2023). Meanwhile, flux is likely primarily driven by a compromised methane filter, evidenced by a salinity driven decrease in MOB and ANME richness and diversity (**Section 4.2.3**). Considering that salinisation is expected to increase with reduced freshwater flows in the future (Tweedley et al. 2019), it is important that high productivity systems account for methane emissions within carbon budgets, regardless of salinity.

5.1 Atmospheric methane flux rates across a salinity gradient

Overall atmospheric methane fluxes did not differ greatly across the salinity gradient in the Coorong and lower lakes. These results are contrary to many global studies, where salinity is often a primary predictor of atmospheric methane flux (Poffenbarger et al. 2011; Zhou et al. 2022), albeit across contracted estuarine salinity gradients. Hypersaline lakes have recorded flux rates of 2.64 - 2.88 mg methane m^{-2} d^{-1} (Gar'kusha et al. 2025), whereas within hypersaline coastal lagoons characterised by seagrass meadows, rates ranged from 0.19 - 13.09 mg methane m^{-2} d^{-1} (Yu et al. 2024). The recorded flux rates in the Coorong's were variable, but often higher (0.68 - 45.8 mg methane m^{-2} d^{-1}).

When considering the Coorong and Lower lakes flux rates globally, they rival other productive coastal systems (**Table 4**). Median flux rates are comparable to salt marshes globally, and significantly higher than other coastal systems. Although no global estimates have been achieved for hypersaline systems, which are expected to increase in prevalence and extent as salinisation of aquatic systems increases (Keneally et al. 2025)

Table 4: Total annual methane emissions from aquatic environments compiled from global estimates of Rosentreter et al. (2021). Coorong upscaled estimates were conducted assuming a constant flux rate. Rosentreter et al. (2021) did not include any hypersaline systems within their review.

Water body	Median Rate (mg CH_4 m^{-2} d^{-1})	Reference
Global Estimates (total)		
Estuaries	0.61	From Rosentreter et al. (2021)
Salt marshes	8.75	
Mangroves	4.25	
Seagrasses	1.30	
Tidal flats	3.62	
Lakes	48.5	
Region Estimates		
Coorong & Lower Lakes	**8.44**	This study

Measured flux rates of September were in line with modelled diffusive fluxes (**Appendix C; Figure S3**), although July rates were substantially higher. Differences between floating chamber and boundary layer methods (BLM) of deriving fluxes are common, due to varying and hard to account for temporal coverage (frequency of water column sampling for BLM & deployment times for floating chambers) (Erkkilä et al. 2018; Podgrajsek et al. 2014).

With methane flux rates being relatively consistent across salinity, there appears to be high heterogeneity in flux drivers in the Coorong and Lower Lakes. It is evident that methane flux is driven by a range of site- and salinity-specific processes. These include;

a) physical processes (e.g. mixing & flow), **b) chemical processes** (e.g. solubility & gas interactions), and **C) biological interactions** (e.g. production and oxidation pathways, competition, and predator-prey microbial dynamics). Hence to fully account for methane across salinity gradients, an in-depth understanding of the interactions between these processes must be further developed across the salinity gradient.

5.2 Physical and chemical constraints on methane flux

5.2.1 Biogeochemical characterisation of the study sites

The concentrations of key compounds in the pore water (i.e. CH_4, SO_4^{2-}, H_2S & OM) were within the range of previously recorded data within the Coorong and lower lakes (Keneally et al. 2024, Mosley et al. 2024, Huang et al. 2025 & Mosley et al. 2014). Sulfate is generally depleted within surface sediments due to SRB (Berner 1980). Although, no significant trends were observed within sulfate profiles likely due to carbon limitation relative to the accumulated sulfate, which can be observed in other hypersaline systems (Krause & Treude 2021 & Liu et al. 2024).

Dissolved sulfide was also enriched within hypersaline sites, close to where monosulfidic black oozes (MBOs) are commonly observed (Mosely et al. 2021). While sulfate was heavily reduced at brackish sites compared to hypersaline sites, dissolved sulfide was equivalent (65.94 - 238.23 μM H_2S). Here, the rate of sulfate reduction and subsequent sulfide export (through consumption or volatilisation and oxidation) is likely higher in hypersalinity than brackish conditions. As mentioned, MBOs form regularly within the Coorong, as a function of its eutrophication driven high organic carbon deposition, and

subsequent anoxic sediments (Mosley et al. 2022). Hence dissolved sulfide is likely being produced faster, but transported into monosulfidic compounds, which are not measured on passive DGT samplers.

Methane within hypersaline sediments was generally low, but higher than previously measured in the Coorong, likely due to the warmer temperatures during sampling (Keneally et al. 2024). Higher methane concentrations were found in organic rich surface sediments, but concentration reduced with sediment depth. This is similar to observations in other coastal sediments with high organic matter deposition rates (Egger et al. 2016; Xiao et al. 2017). At brackish and freshwater sites methane concentrations approached but did not reach supersaturation, which is the requirement for bubble formation and ebullition (Boudreau et al. 2005). Methane supersaturation is common across freshwater and coastal system but is often observed deeper within the sediment than was sampled for in this study (Tyroller et al. 2016; Sobek et al. 2012; McGinnis et al. 2015). Further undersaturation could occur due to sampling procedure artifacts such as the disruption of surface sediments, resulting in degassing (Sollberger et al. 2014).

For each of the saline sites, it is suspected that the SMTZ is within the surface sediments, and even thinner for hypersaline sites. Shoaling of the SMTZ is common within high organic matter burial environments, and synonymous with intense eutrophication (Egger et al. 2017; Myllykangas et al. 2020). Additionally, shoaling shortens the diffusive path of methane to the water column, resulting in higher sediment diffusion rates (**figure 3**) (Myllykangas et al. 2020).

Sediment conditions reflected similar hypersaline systems globally. Porewater methane within hypersaline sediments varied from 1.54 - 62.24 µM within this study. Within inland hypersaline lakes porewater methane can vary from 47 - 163 µM (Gar'kusha et al. 2025). Coastal hypersaline wetlands were found to be within 10 - 50 µM methane (Krause & Treude 2021 & Liu et al. 2024).

Flux is likely dominated by diffusive pathways due to sediment shoaling within brackish and hypersaline sites. Additionally, increasing salinity significantly reduces methane solubility, with solubility at hypersaline sites being roughly half of freshwater (Wiesenburg & Guinasso, 1979). Ebullition which has been documented as the primary flux pathway from shallow systems (Weber et al. 2019; Chuang et al. 2017) was not detected despite using methods to differentiate diffusion from ebullition as per Sø et al. (2024). Hence, the reduced solubility of methane at hypersaline sites can enhance gas transfer by promoting a greater tendency for methane to escape to the atmosphere through diffusion (Wiesenburg & Guinasso, 1979; Wanninkhof, 1992). These findings contrast traditional methane dynamics of sediment storage, potentially making atmospheric flux rates more tied to sediment production. While possible from brackish and fresh sites in the Coorong, ebullition was not captured during sampling, hence fluxes may be significantly underestimated. Ebullition could be confirmed in the future through the use of bubble traps (Gao et al. 2013).

5.2.2 Physical constraints

With gas diffusion identified as the primary flux pathway within this study, a range of physical constraints can influence the fate of methane. It becomes difficult to spatially relate measured methane fluxes with other samples when significant mixing or flow

occurs (Liu et al. 2021). This is particularly relevant for the GB site, where intermittent flow from the upstream barrage combined with tidal influence from the Murray Mouth likely makes the site an organic matter depositional zone due to high sediment residence times. Similarly, sites such as SC experienced notable flow from a nearby freshwater creek (Tilley Swap Drain), which may have interfered with flux measurements.

Sediment porosity is a key limiting factor in sediment diffusion rates, with more porous sediments facilitating faster diffusion (Judd & Hovland 1992). In freshwater sites where methane generation occurs at greater depths, low porosity may slow diffusion, thereby reducing sediment flux rates as compared to sediment surface production at hypersaline sites.

Wind shear is likely the predominant driver of gas flux in the Coorong (MacIntyre et al. 2010), as the shallow, well-mixed water column likely exhibits minimal buoyancy flux (Chilton 2024). Consequently, turbulence generated by wind stress is likely the main factor enhancing gas transfer, given the limited thermal stratification that would otherwise dampen surface turbulence (MacIntyre et al. 2002). As a result, sediment diffusion rates may be closely coupled to atmospheric exchange due to the depth of wind-driven turbulence. Wind effects are also evident in the spatial patterns of organic deposition, with frequent wind-induced waves and current-driven resuspension of fine benthic particles observed within the Coorong (Chilton 2024; Keneally et al. 2024). These processes often erode shoreline areas, transporting fine sediments to deeper zones that support high productivity (Chilton 2024). Consequently, organic depositional zones form, creating strongly reducing and competitive sediment environments (Keneally et al.

2024). Wind-induced shear stress on sediments may further increase methane diffusion rates, although this relationship has primarily been documented for ebullition (Joyce 2003).

5.3 Microbial community shifts in methane generation and consumption

Microbial analyses revealed that salinity is a key driver of community structure, acting as a critical environmental filter across site, regional, and global scales (Caporaso et al. 2011; Keneally et al. *In Review*; Song et al. 2022).

5.3.1 Methanogenic pathway changes

Methanogen α-diversity indicated an expected community response to salinity as an environmental filter. As salinity increased methanogen richness decreased, but a more even distribution among taxa was observed (**Figure 7A**). Salinity is acting as an environmental filter, removing rare taxa that cannot cope under high stress (Caporaso et al. 2011).

Additionally, methanogen β-diversity indicated clear groupings between salinity categories, similar to whole community bacterial and archaeal β-diversity. Methanogenic Archaea possess flexible metabolisms, able to metabolise a wide range of substrates (Kurth et al. 2020). Hence as salinity increases, methanogenesis can be facilitated through the utilisation of alternative metabolic pathways (McGenity 2010). This is further exemplified in the identified pathways from both conservative and predictive function classifying databases (**Figure 9 & A4**).

Within hypersaline environments, microbes are required to maintain a high internal osmotic pressure through osmoadaptation, accumulating ions and specific organic solutes (Gregory and Boyd 2021). Many of these osmolytes come in the form of methylated compounds, or precursors to methylated compounds (e.g. Glycine Betaine) (Welsh 2000; Boysen et al. 2022). Additionally, many of these compounds can be non-competitive (fermentation of glycine betaine into trimethylamine) (Welsh 2000). Hence, osmolyte driven methylotrophic methanogenesis is likely to be the predominate pathway of methanogenesis in hypersaline sediments. These results align with recent studies finding methylotrophic methanogenesis within hypersaline depositional zones in the Coorong (Keneally et al. 2024).

Within freshwater and brackish sites hydrogenotrophic and acetoclastic pathways are the dominate forms of methanogenesis. Without competition from SRB, methanogens have significantly enhanced access to a range of more preferrable substrates, hence suggesting these pathways (Li et al. 2023).

5.3.2 Constraints on methane oxidation

Analysis of methanotrophic communities revealed a significant decrease in richness, and Shannon diversity as salinity increases for both MOB, and ANME. Hypersaline sites showed the most significant decrease in ANME having almost no identified taxa. ANME have been identified in hypersaline systems globally in sediments involved in cryptic methane cycling (Liu et al. 2024; Krause et al. 2023). Recent studies have shown no significant salinity stress in the case of ANME such as '*Candidatus Methanoperedens nitroreducens*', although this relationship has not been explored thoroughly for other

species (Frank et al. 2023; Nauhaus et al. 2005). ANME β-diversity revealed salinity as its strongest predictor, although this may have been due to other site characteristics.

ANME are known to be an extremely slow growing organism, taking up to 60 years to establish a steady-state AOM biomass (Timmers et al. 2015). In cases of high sedimentation rates, the residence time for microbial communities can be limited (Thang et al. 2013), meaning the slow growth rate of ANME may not be able to keep up with sedimentation. Wind-induced sheer stress on surface sediments in shallow (<1m depth; Chilton et al. 2024) sites, paired with constant changes in salinity, may further limit the growth of AOM, although this has not been specifically investigated through the literature. Hence, their absence may not be a function of only salinity stress, but instead of multiple convergent physical processes.

Although sulfide toxicity to ANME is well documented (Timmers et al., 2015; Dalcin Martins et al., 2024), it appears to be insignificant in the Coorong, where ANME are most prevalent under brackish conditions. Previous studies which have observed dissolved sulfide toxicity have been implicated in significantly higher concentrations (up to 4 mM) which are unlikely to occur within the Coorong due to monosulfidic material formation (Mosley et al. 2022).

In hypersaline sites, the absence of ANME suggests that the sediment microbial filter is severely compromised. This may help explain why calculated sediment diffusion rates differ greatly from measured atmospheric fluxes at brackish sites, where the ANME-mediated filter remains. In contrast, at freshwater sites, the deeper methanogenic zone

allows for significant AOM, contributing to a steep decline in methane before it reaches the surface water interface. Such results support recent suggestions of the importance of microbially-informed biogeochemical investigations to better understand and predict important ecosystem processes (Wallenius et al 2021; Reed et al. 2014; Keneally et al. 2025).

MOB exhibited a decrease in both diversity and richness however, unlike ANME, a notable abundance of taxa was still observed in hypersaline sites. β-diversity PERMANOVA analysis indicated that salinity is a key driver of MOB distribution, in which they are known to exhibit some degree of salinity stress (Ho et al. 2018; Zhang et al. 2023). As salinity increases, MOB diversity declines and overall community composition shifts. As conditions become more extreme, specialists are favoured such as putative thermophiles (*Methylocaldum*), acidophiles (*Methylosoma*), and haloalkaliphiles (*Methylomicrobium*) (Sherry et al. 2016). Additionally, MOB have been shown to be less sensitive to gradual changes in salinity compared to sudden shifts, which can trigger significant successional processes (Osudar et al. 2017). Hence, while salinity decreases methanotroph diversity, an active filter layer of MOB are likely active within hypersaline waters and oxygenated surface sediments, although less diverse and abundant than fresher sites. It is also important to note that these observations were derived from sediment samples, meaning the data represent deposited MOB rather than active communities within the water column.

6.0 The fate of methane across salinity gradients

It is evident that while salinity may not directly change measured flux rates, it significantly changes the processes resulting in atmospheric methane flux (**Figure 10**). These processes, and a mixture of physical, chemical and biological components differ greatly between sites, making it difficult to estimate methane flux. Primarily, as salinity increases, methanogenic communities shift to metabolise methylated substrates within organic matter depositional zones. Produced methane can be transported to the atmosphere through a shortened diffusion path, lack of sedimentary microbial filter and reduced aerobic microbial filter, hence driving comparible fluxes across the broad salinity gradient.

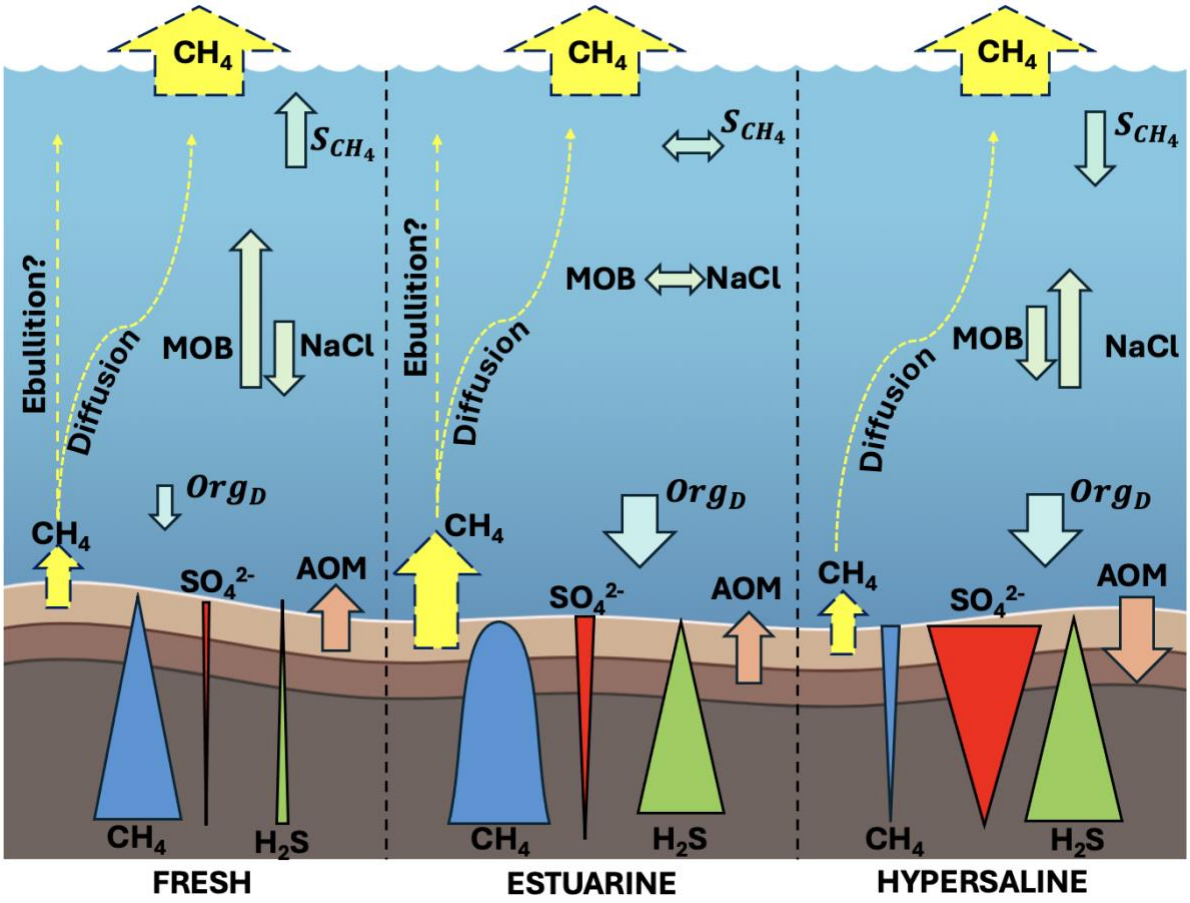

Figure 6: Conceptual model of the changes in methane cycling processes across three salinity categories. Here, MOB represents methane oxidising bacteria, AOM

represents the anerobic oxidation of methane, CH_4 represents methane, SO_4^{2-} represent sulfate, H_2S represents dissolved sulfide, Org_D represents organic matter deposition & S_{CH_4} represents methane solubility.

These controls on methane flux in hypersaline systems are not well described globally and present an important gap in the current understanding of aquatic methane emissions. To effectively account for carbon emissions, and thereafter influence policy, the rates and processes coming from hypersaline systems must be better constrained. As salinisation is expected to increase in the future, it is essential that methane cycling, and each of the outlined processes are investigated and quantified, to build a holistic understanding of the drivers of flux across broad salinity gradients.

References:

Anderson, MJ & Walsh, DCI 2013, 'PERMANOVA, ANOSIM, and the Mantel test in the face of heterogeneous dispersions: What null hypothesis are you testing?', *Ecological Monographs*, vol. 83, no. 4, 2013/11/01, pp. 557-574.

Bastviken, D, Nygren, J, Schenk, J, Parellada Massana, R & Duc, NT 2020, 'Technical note: Facilitating the use of low-cost methane (CH4) sensors in flux chambers – calibration, data processing, and an open-source make-it-yourself logger', *Biogeosciences*, vol. 17, no. 13, pp. 3659-3667.

Beaulieu, JJ, DelSontro, T & Downing, JA 2019, 'Eutrophication will increase methane emissions from lakes and impoundments during the 21st century', *Nature Communications*, vol. 10, no. 1, 2019/03/26, p. 1375.

Berner, RA 1980, *Early Diagenesis: A Theoretical Approach*, Princeton University Press.

Boudreau, BP, Algar, C, Johnson, BD, Croudace, I, Reed, A, Furukawa, Y, Dorgan, KM, Jumars, PA, Grader, AS & Gardiner, BS 2005, 'Bubble growth and rise in soft sediments', *Geology*, vol. 33, no. 6, pp. 517-520.

Bricker, SB 1999, 'National estuarine eutrophication assessment: effects of nutrient enrichment in the nation's estuaries'.

Bridgham, SD, Cadillo-Quiroz, H, Keller, JK & Zhuang, Q 2013, 'Methane emissions from wetlands: biogeochemical, microbial, and modeling perspectives from local to global scales', *Global Change Biology*, vol. 19, no. 5, 2013/05/01, pp. 1325-1346.

Chilton, D, 2024, Wind-induced sediment resuspension in the Coorong, a shallow estuarine lagoon degraded by modifications to its freshwater flow regime

Chilton, D, Hamilton, DP, Nagelkerken, I, Cook, P, Hipsey, MR, Reid, R, Sheaves, M, Waltham, NJ & Brookes, J 2021, 'Environmental Flow Requirements of Estuaries: Providing Resilience to Current and Future Climate and Direct Anthropogenic Changes', *Frontiers in Environmental Science*, vol. Volume 9 - 2021, 2021-November-17.

Chuang, PC, Young, MB, Dale, AW, Miller, LG, Herrera-Silveira, JA & Paytan, A 2017, 'Methane fluxes from tropical coastal lagoons surrounded by mangroves, Yucatán, Mexico', *Journal of Geophysical Research: Biogeosciences*, vol. 122, no. 5, 2017/05/01, pp. 1156-1174.

Dalcin Martins, P, de Monlevad, JPRC, Echeveste Medrano, MJ, Lenstra, WK, Wallenius, AJ, Hermans, M, Slomp, CP, Welte, CU, Jetten, MSM & van Helmond, NAGM 2024, 'Sulfide Toxicity as Key Control on Anaerobic Oxidation of Methane in Eutrophic

Coastal Sediments', *Environmental science & technology*, vol. 58, no. 26, 2024/07/02, pp. 11421-11435.

Douglas, GM, Maffei, VJ, Zaneveld, JR, Yurgel, SN, Brown, JR, Taylor, CM, Huttenhower, C & Langille, MGI 2020, 'PICRUSt2 for prediction of metagenome functions', *Nature Biotechnology*, vol. 38, no. 6, 2020/06/01, pp. 685-688.

Egger, M, Lenstra, W, Jong, D, Meysman, FJR, Sapart, CJ, van der Veen, C, Röckmann, T, Gonzalez, S & Slomp, CP 2016, 'Rapid Sediment Accumulation Results in High Methane Effluxes from Coastal Sediments', *PLOS ONE*, vol. 11, no. 8, p. e0161609.

El-Fadel, M & Massoud, M 2001, 'Methane emissions from wastewater management', *Environmental Pollution*, vol. 114, no. 2, 2001/09/01/, pp. 177-185.

Erkkilä, KM, Ojala, A, Bastviken, D, Biermann, T, Heiskanen, JJ, Lindroth, A, Peltola, O, Rantakari, M, Vesala, T & Mammarella, I 2018, 'Methane and carbon dioxide fluxes over a lake: comparison between eddy covariance, floating chambers and boundary layer method', *Biogeosciences*, vol. 15, no. 2, pp. 429-445.

Frank, J, Zhang, X, Marcellin, E, Yuan, Z & Hu, S 2023, 'Salinity effect on an anaerobic methane- and ammonium-oxidising consortium: Shifts in activity, morphology, osmoregulation and syntrophic relationship', *Water Research*, vol. 242, 2023/08/15/, p. 120090.

Gao, Y, Liu, X, Yi, N, Wang, Y, Guo, J, Zhang, Z & Yan, S 2013, 'Estimation of N2 and N2O ebullition from eutrophic water using an improved bubble trap device', *Ecological Engineering*, vol. 57, 2013/08/01/, pp. 403-412.

Gar'kusha, D, Fedorov, Y, Ovsepyan, A, Popov, Y, Andreev, Y, Talpa, B, Tambieva, N & Myakinnikov, I 2025, 'Carbon Dioxide and Methane Emission into the Atmosphere and Its Relationship with Chemogenic Sedimentation in the Hypersaline Lake Baskunchak (Russia)', *Water*, vol. 17, no. 5, DOI 10.3390/w17050738.

Håkanson, L & Jansson, M 2002, *Principles of Lake Sedimentology*.

Hermans, M, Stranne, C, Broman, E, Sokolov, A, Roth, F, Nascimento, FJA, Mörth, C-M, ten Hietbrink, S, Sun, X, Gustafsson, E, Gustafsson, BG, Norkko, A, Jilbert, T & Humborg, C 2024, 'Ebullition dominates methane emissions in stratified coastal waters', *Science of The Total Environment*, vol. 945, 2024/10/01/, p. 174183.

Ho, A, Mo, Y, Lee, HJ, Sauheitl, L, Jia, Z & Horn, MA 2018, 'Effect of salt stress on aerobic methane oxidation and associated methanotrophs; a microcosm study of a natural community from a non-saline environment', *Soil Biology and Biochemistry*, vol. 125, pp.

Hopkinson, CS, Buffam, I, Hobbie, J, Vallino, J, Perdue, M, Eversmeyer, B, Prahl, F, Covert, J, Hodson, R, Moran, MA, Smith, E, Baross, J, Crump, B, Findlay, S & Foreman, K 1998, 'Terrestrial inputs of organic matter to coastal ecosystems: An intercomparison of

chemical characteristics and bioavailability', *Biogeochemistry*, vol. 43, no. 3, 1998/12/01, pp. 211-234.

Huang, J, Lam-Gordillo, O, Mosley, LM, Keneally, C, Brookes, J & Welsh, DT 2025, 'Understanding sediment nutrient cycling in a hypersaline coastal lagoon using hydrogel-based passive sampling techniques', *Marine Pollution Bulletin*, vol. 214, 2025/05/01/, p. 117714.

Imberger, J 1985, 'The diurnal mixed layer', *Limnology and Oceanography*, vol. 30, no. 4, pp. 737-770.

IPCC, 2014. Synthesis Report. Contribution of working groups I. II and III to the fifth assessment report of the intergovernmental panel on climate change 151

Jackson, RB, Saunois, M, Bousquet, P, Canadell, JG, Poulter, B, Stavert, AR, Bergamaschi, P, Niwa, Y, Segers, A & Tsuruta, A 2020, 'Increasing anthropogenic methane emissions arise equally from agricultural and fossil fuel sources', *Environmental Research Letters*, vol. 15, no. 7, 2020/07/15, p. 071002.

Jähne, B, Münnich, KO, Bösinger, R, Dutzi, A, Huber, W & Libner, P 1987, 'On the parameters influencing air-water gas exchange', *Journal of Geophysical Research: Oceans*, vol. 92, no. C2, 1987/02/15, pp. 1937-1949.

Jeppesen, E, Beklioğlu, M, Özkan, K & Akyürek, Z 2020, 'Salinization Increase due to Climate Change Will Have Substantial Negative Effects on Inland Waters: A Call for Multifaceted Research at the Local and Global Scale', *The Innovation*, vol. 1, no. 2.

Johnson K, Hughes J, Donaghay P, Sieburth J (1990) 'Bottle-calibration static head space method for the determination of methane dissolved in seawater' *Analytical Chemistry,* 62**,** 2408-2412.

Johnson, KA & Johnson, DE 1995, 'Methane emissions from cattle', *Journal of Animal Science*, vol. 73, no. 8, pp. 2483-2492.

Joyce, J 2003, 'Physical Controls on Methane Ebullition from Reservoirs and Lakes', *Environmental & Engineering Geoscience*, vol. 9, May 01, 2003, pp. 167-178.
Judd, AG & Hovland, M 1992, 'The evidence of shallow gas in marine sediments', *Continental Shelf Research*, vol. 12, no. 10, 1992/10/01/, pp. 1081-1095.

Keneally, C, Chilton, D, Dornan, TN, Kidd, SP, Gaget, V, Toomes, A, Lassaline, C, Petrovski, R, Wood, L & Brookes, JD 2025, 'Multi-omics reveal microbial succession and metabolomic adaptations to flood in a hypersaline coastal lagoon', *Water Research*, vol. 280, 2025/07/15/, p. 123511.

Keneally, C, Gaget, V, Chilton, D, Kidd, SP, Mosley, L, Welsh, DT, Zhou, Y, Zhou, L & Brookes, J 2025, 'Microbial ecology in hypersaline coastal lagoons: A model for climate-induced coastal salinisation and eutrophication', *Earth-Science Reviews*, vol. 266, 2025/07/01/, p. 105150.

Keneally, C, Southgate, M, Chilton, D, Gaget, V, Welsh, DT, Mosley, L, Erler, DV, Kidd, SP & Brookes, J 2024, 'Organic matter accumulation drives methylotrophic methanogenesis and microbial ecology in a hypersaline coastal lagoon', *Limnology and Oceanography*, vol. n/a, no. n/a, 2024/07/20.

Keneally, C., Gaget, V., Chilton, D., Dornan, T.N., Hensel, J., Keneally, A., Kidd, S.P., Brookes, J.D., In Review. Specialist–generalist trade-offs structure sediment microbial community assembly and interactions along an extreme salinity gradient. Environmental Microbiology Reports

Krause, SJE & Treude, T 2021, 'Deciphering cryptic methane cycling: Coupling of methylotrophic methanogenesis and anaerobic oxidation of methane in hypersaline coastal wetland sediment', *Geochimica et Cosmochimica Acta*, vol. 302, 2021/06/01/, pp. 160-174.

Krause, SJE, Liu, J, Yousavich, DJ, Robinson, D, Hoyt, DW, Qin, Q, Wenzhöfer, F, Janssen, F, Valentine, DL & Treude, T 2023, 'Evidence of cryptic methane cycling and non-methanogenic methylamine consumption in the sulfate-reducing zone of sediment in the Santa Barbara Basin, California', *Biogeosciences*, vol. 20, no. 20, pp. 4377-4390.

Kurth, JM, Op den Camp, HJM & Welte, CU 2020, 'Several ways one goal—methanogenesis from unconventional substrates', *Applied Microbiology and Biotechnology*, vol. 104, no. 16, 2020/08/01, pp. 6839-6854.

Large, WG & Pond, S 1981, 'Open Ocean Momentum Flux Measurements in Moderate to Strong Winds', *Journal of Physical Oceanography*, vol. 11, March 01, 1981, pp. 324-336.

Le Moal, M, Gascuel-Odoux, C, Ménesguen, A, Souchon, Y, Étrillard, C, Levain, A, Moatar, F, Pannard, A, Souchu, P, Lefebvre, A & Pinay, G 2019, 'Eutrophication: A new wine in an old bottle?', *Science of The Total Environment*, vol. 651, 2019/02/15/, pp. 1-11.

Li, B, Wang, H, Lai, A, Xue, J, Wu, Q, Yu, C, Xie, K, Mao, Z, Li, H, Xing, P & Wu, QL 2023, 'Hydrogenotrophic pathway dominates methanogenesis along the river-estuary continuum of the Yangtze River', *Water Research*, vol. 240, 2023/07/15/, p. 120096.

Liss, PS & Slater, PG 1974, 'Flux of Gases across the Air-Sea Interface', *Nature*, vol. 247, no. 5438, 1974/01/01, pp. 181-184.

Liu, J, Klonicki-Ference, E, Krause, SJE & Treude, T 2025, 'Iron Oxides Fuel Anaerobic Oxidation of Methane in the Presence of Sulfate in Hypersaline Coastal Wetland Sediment', *Environmental science & technology*, vol. 59, no. 1, 2025/01/14, pp. 513-522.

Liu, J, Xiao, S, Wang, C, Yang, Z, Liu, D, Guo, X, Liu, L & Lorke, A 2021, 'Spatial and temporal variability of dissolved methane concentrations and diffusive emissions in the Three Gorges Reservoir', *Water Research*, vol. 207, 2021/12/01/, p. 117788.

Lovley, DR & Klug, MJ 1983, 'Sulfate reducers can outcompete methanogens at freshwater sulfate concentrations', *Appl Environ Microbiol*, vol. 45, no. 1, Jan, pp. 187-192.

Louca, S, Parfrey, LW & Doebeli, M 2016, 'Decoupling function and taxonomy in the global ocean microbiome', *Science*, vol. 353, no. 6305, 2016/09/16, pp. 1272-1277.

Love, MI, Huber, W & Anders, S 2014, 'Moderated estimation of fold change and dispersion for RNA-seq data with DESeq2', *Genome Biology*, vol. 15, no. 12, 2014/12/05, p. 550.

MacIntyre, S, Eugster, W & Kling, GW 2002, 'The critical importance of buoyancy flux for gas flux across the air-water interface', *Geophysical Monograph-American Geophysical Union*, vol. 127, pp. 135-140.

MacIntyre, S, Jonsson, A, Jansson, M, Aberg, J, Turney, DE & Miller, SD 2010, 'Buoyancy flux, turbulence, and the gas transfer coefficient in a stratified lake', *Geophysical Research Letters*, vol. 37, no. 24, 2010/12/01.

Magen, C, Lapham, LL, Pohlman, JW, Marshall, K, Bosman, S, Casso, M & Chanton, JP 2014, 'A simple headspace equilibration method for measuring dissolved methane', *Limnology and Oceanography: Methods*, vol. 12, no. 9, 2014/09/01, pp. 637-650.

McGenity, TJ 2010, 'Methanogens and Methanogenesis in Hypersaline Environments', in KN Timmis (ed.), *Handbook of Hydrocarbon and Lipid Microbiology*, Springer Berlin Heidelberg, Berlin, Heidelberg, pp. 665-680.

McGinnis, DF, Kirillin, G, Tang, KW, Flury, S, Bodmer, P, Engelhardt, C, Casper, P & Grossart, H-P 2015, 'Enhancing Surface Methane Fluxes from an Oligotrophic Lake: Exploring the Microbubble Hypothesis', *Environmental science & technology*, vol. 49, no. 2, 2015/01/20, pp. 873-880.

Menéndez-Serra, M, Triadó-Margarit, X, Castañeda, C, Herrero, J & Casamayor, EO 2019, 'Microbial composition, potential functional roles and genetic novelty in gypsum-rich and hypersaline soils of Monegros and Gallocanta (Spain)', *Science of The Total Environment*, vol. 650, 2019/02/10/, pp. 343-353.

Middelburg, J & Levin, L 2009, 'Coastal hypoxia and sediment biogeochemistry', *Biogeosciences Discussions*, vol. 6, 07/28.

Mosley L, Farkas J, Shao Y, and Fitzpatrick R (2022). Monosulfidic Black Ooze (MBO) formation, cycling and management in the Coorong. University of Adelaide technical report.

Mosley, LM, Shand, P, Self, P & Fitzpatrick, R 2014, 'The geochemistry during management of lake acidification caused by the rewetting of sulfuric (pH<4) acid sulfate soils', *Applied Geochemistry*, vol. 41, 2014/02/01/, pp. 49-61.

Myllykangas, J-P, Hietanen, S & Jilbert, T 2020, 'Legacy Effects of Eutrophication on Modern Methane Dynamics in a Boreal Estuary', *Estuaries and Coasts*, vol. 43, no. 2, 2020/03/01, pp. 189-206.

Nauhaus, K, Treude, T, Boetius, A & Krüger, M 2005, 'Environmental regulation of the anaerobic oxidation of methane: a comparison of ANME-I and ANME-II communities', *Environmental Microbiology*, vol. 7, no. 1, 2005/01/01, pp. 98-106.

Oksanen J, Simpson G, Blanchet F, Kindt R, Legendre P, Minchin P, O'Hara R, Solymos P, Stevens M, Szoecs E, Wagner H, Barbour M, Bedward M, Bolker B, Borcard D, Borman T, Carvalho G, Chirico M, De Caceres M, Durand S, Evangelista H, FitzJohn R, Friendly M, Furneaux B, Hannigan G, Hill M, Lahti L, Martino C, McGlinn D, Ouellette M, Ribeiro Cunha E, Smith T, Stier A, Ter Braak C, Weedon J 2025, 'vegan: Community Ecology Package.' R package version 2.8-0, https://vegandevs.github.io/vegan/.

Osudar, R, Klings, KW, Wagner, D & Bussmann, I 2017, 'Effect of salinity on microbial methane oxidation in freshwater and marine environments', *Aquatic Microbial Ecology*, vol. 80, pp. 181-192.

Podgrajsek, E, Sahlée, E & Rutgersson, A 2014, 'Diurnal cycle of lake methane flux', *Journal of Geophysical Research: Biogeosciences*, vol. 119, no. 3, pp. 236-248.

Poffenbarger, HJ, Needelman, BA & Megonigal, JP 2011, 'Salinity Influence on Methane Emissions from Tidal Marshes', *Wetlands*, vol. 31, no. 5, 2011/10/01, pp. 831-842.

R Core Team 2024, 'R: A Language and Environment for Statistical Computing', *R Foundation for Statistical Computing*, Vienna, Austria. <https://www.R-project.org/>.

Robertson, D, Teasdale, PR & Welsh, DT 2008, 'A novel gel-based technique for the high resolution, two-dimensional determination of iron (II) and sulfide in sediment', *Limnology and Oceanography: Methods*, vol. 6, no. 10, 2008/10/01, pp. 502-512.

Rosentreter, JA, Alcott, L, Maavara, T, Sun, X, Zhou, Y, Planavsky, NJ & Raymond, PA 2024, 'Revisiting the Global Methane Cycle Through Expert Opinion', *Earth's Future*, vol. 12, no. 6, 2024/06/01, p. e2023EF004234.

Rosentreter, JA, Borges, AV, Deemer, BR, Holgerson, MA, Liu, S, Song, C, Melack, J, Raymond, PA, Duarte, CM, Allen, GH, Olefeldt, D, Poulter, B, Battin, TI & Eyre, BD 2021, 'Half of global methane emissions come from highly variable aquatic ecosystem sources', *Nature Geoscience*, vol. 14, no. 4, 2021/04/01, pp. 225-230.

Rosentreter, JA, Maher, DT, Erler, DV, Murray, RH & Eyre, BD 2018, 'Methane emissions partially offset "blue carbon" burial in mangroves', *Science Advances*, vol. 4, no. 6, p. eaao4985.

Sander, R, Acree, WE, Visscher, AD, Schwartz, SE & Wallington, TJ 2022, 'Henry's law constants (IUPAC Recommendations 2021)', *Pure and Applied Chemistry*, vol. 94, no. 1, pp. 71-85.

Saunois, M, Stavert, AR, Poulter, B, Bousquet, P, Canadell, JG, Jackson, RB, Raymond, PA, Dlugokencky, EJ, Houweling, S, Patra, PK, Ciais, P, Arora, VK, Bastviken, D, Bergamaschi, P, Blake, DR, Brailsford, G, Bruhwiler, L, Carlson, KM, Carrol, M, Castaldi, S, Chandra, N, Crevoisier, C, Crill, PM, Covey, K, Curry, CL, Etiope, G, Frankenberg, C, Gedney, N, Hegglin, MI, Höglund-Isaksson, L, Hugelius, G, Ishizawa, M, Ito, A, Janssens-Maenhout, G, Jensen, KM, Joos, F, Kleinen, T, Krummel, PB, Langenfelds, RL, Laruelle, GG, Liu, L, Machida, T, Maksyutov, S, McDonald, KC, McNorton, J, Miller, PA, Melton, JR, Morino, I, Müller, J, Murguia-Flores, F, Naik, V, Niwa, Y, Noce, S, O'Doherty, S, Parker, RJ, Peng, C, Peng, S, Peters, GP, Prigent, C, Prinn, R, Ramonet, M, Regnier, P, Riley, WJ, Rosentreter, JA, Segers, A, Simpson, IJ, Shi, H, Smith, SJ, Steele, LP, Thornton, BF, Tian, H, Tohjima, Y, Tubiello, FN, Tsuruta, A, Viovy, N, Voulgarakis, A, Weber, TS, van Weele, M, van der Werf, GR, Weiss, RF, Worthy, D, Wunch, D, Yin, Y, Yoshida, Y, Zhang, W, Zhang, Z, Zhao, Y, Zheng, B, Zhu, Q, Zhu, Q & Zhuang, Q 2020, 'The Global Methane Budget 2000–2017', *Earth Syst. Sci. Data*, vol. 12, no. 3, pp. 1561-1623.

Schmid, M., Tietze, K., Halbwachs, M., Lorke, A., McGinnis, D., & Wüest, A. (2004). How Hazardous Is the Gas Accumulation in Lake Kivu? Arguments for a Risk Assessment in Light of the Nyiragongo Volcano Eruption of 2002. Acta Vulcanologica, 14/15, 115-121.

Schmid, SM, Fügenschuh, B, Kissling, E & Schuster, R 2004, 'Tectonic map and overall architecture of the Alpine orogen', *Eclogae Geologicae Helvetiae*, vol. 97, no. 1, 2004/05/01, pp. 93-117.

Schorn, S, Graf, JS, Littmann, S, Hach, PF, Lavik, G, Speth, DR, Schubert, CJ, Kuypers, MMM & Milucka, J 2024, 'Persistent activity of aerobic methane-oxidizing bacteria in anoxic lake waters due to metabolic versatility', *Nature Communications*, vol. 15, no. 1, 2024/06/21, p. 5293.

Sherry, A, Osborne, KA, Sidgwick, FR, Gray, ND & Talbot, HM 2016, 'A temperate river estuary is a sink for methanotrophs adapted to extremes of pH, temperature and salinity', *Environmental Microbiology Reports*, vol. 8, no. 1, 2016/02/01, pp. 122-131.

Sobek, S, DelSontro, T, Wongfun, N & Wehrli, B 2012, 'Extreme organic carbon burial fuels intense methane bubbling in a temperate reservoir', *Geophysical Research Letters*, vol. 39, no. 1, 2012/01/01.

Soetaert, K., Petzoldt, T., Meysman, F., 2010. Marelac: Tools for aquatic sciences.

Solden, L, Lloyd, K & Wrighton, K 2016, 'The bright side of microbial dark matter: lessons learned from the uncultivated majority', *Current Opinion in Microbiology*, vol. 31, 2016/06/01/, pp. 217-226.

Starai, VJ & Escalante-Semerena, JC 2004, 'Identification of the protein acetyltransferase (Pat) enzyme that acetylates acetyl-CoA synthetase in Salmonella enterica', *J Mol Biol*, vol. 340, no. 5, Jul 23, pp. 1005-1012.

Steward, JS & Lowe, EF 2010, 'General empirical models for estimating nutrient load limits for Florida's estuaries and inland waters', *Limnology and Oceanography*, vol. 55, no. 1, 2010/01/01, pp. 433-445.

Swaney, DP, Scavia, D, Howarth, RW & Marino, RM 2008, 'Estuarine classification and response to nitrogen loading: Insights from simple ecological models', *Estuarine, Coastal and Shelf Science*, vol. 77, no. 2, 2008/04/10/, pp. 253-263.

Tedford, EW, MacIntyre, S, Miller, SD & Czikowsky, MJ 2014, 'Similarity scaling of turbulence in a temperate lake during fall cooling', *Journal of Geophysical Research: Oceans*, vol. 119, no. 8, pp. 4689-4713.

Timmers, PH, Widjaja-Greefkes, HCA, Ramiro-Garcia, J, Plugge, CM & Stams, AJ 2015, 'Growth and activity of ANME clades with different sulfate and sulfide concentrations in the presence of methane', *Frontiers in Microbiology*, vol. Volume 6 - 2015, 2015-September-22.

Themelis, NJ & Ulloa, PA 2007, 'Methane generation in landfills', *Renewable Energy*, vol. 32, no. 7, 2007/06/01/, pp. 1243-1257.

Tweedley, JR, Dittmann, SR, Whitfield, AK, Withers, K, Hoeksema, SD & Potter, IC 2019, 'Chapter 30 - Hypersalinity: Global Distribution, Causes, and Present and Future Effects on the Biota of Estuaries and Lagoons', in E Wolanski, JW Day, M Elliott & R Ramachandran (eds), *Coasts and Estuaries*, Elsevier, pp. 523-546.

Tyroller, L, Tomonaga, Y, Brennwald, MS, Ndayisaba, C, Naeher, S, Schubert, C, North, RP & Kipfer, R 2016, 'Improved Method for the Quantification of Methane Concentrations in Unconsolidated Lake Sediments', *Environmental science & technology*, vol. 50, no. 13, 2016/07/05, pp. 7047-7055.

Wallenius, AJ, Dalcin Martins, P, Slomp, CP & Jetten, MSM 2021, 'Anthropogenic and Environmental Constraints on the Microbial Methane Cycle in Coastal Sediments', *Frontiers in Microbiology*, vol. 12.

Wanninkhof, R 1992, 'Relationship between wind speed and gas exchange over the ocean', *Journal of Geophysical Research: Oceans*, vol. 97, no. C5, 1992/05/15, pp. 7373-7382.

Weber, T, Wiseman, NA & Kock, A 2019, 'Global ocean methane emissions dominated by shallow coastal waters', *Nature Communications*, vol. 10, no. 1, 2019/10/08, p. 4584.

Weiss R, Price B (1980) 'Nitrous oxide solubility in water and seawater' *Marine Chemistry*, **8**(4), pp.347-359.

Weiss, RF 1974, 'Carbon dioxide in water and seawater: the solubility of a non-ideal gas', *Marine Chemistry*, vol. 2, no. 3, 1974/11/01/, pp. 203-215.

Wiesenburg, DA & Guinasso, NL, Jr. 1979, 'Equilibrium solubilities of methane, carbon monoxide, and hydrogen in water and sea water', *Journal of Chemical & Engineering Data*, vol. 24, no. 4, 1979/10/01, pp. 356-360.

Wilhelm, E, Battino, R & Wilcock, R 1977, 'Low-Pressure Solubility of Gases in Liquid Water', *Chemical Reviews - CHEM REV*, vol. 77, 04/01.

Xiao, K-Q, Beulig, F, Kjeldsen, KU, Jørgensen, BB & Risgaard-Petersen, N 2017, 'Concurrent Methane Production and Oxidation in Surface Sediment from Aarhus Bay, Denmark', *Frontiers in Microbiology*, vol. Volume 8 - 2017, 2017-June-30.

Yang, C, Mai, J, Cao, X, Burberry, A, Cominelli, F & Zhang, L 2023, 'ggpicrust2: an R package for PICRUSt2 predicted functional profile analysis and visualization', *Bioinformatics*, vol. 39, no. 8, p. btad470.

Yu, H, Coffin, R & Organ, H 2024, 'Dynamics of methane emissions from northwestern Gulf of Mexico subtropical seagrass meadows', *Biogeochemistry*, vol. 167, no. 5, 2024/05/01, pp. 723-741.

Zhang, S, Yan, L, Cao, J, Wang, K, Luo, Y, Hu, H, Wang, L, Yu, R, Pan, B, Yu, K, Zhao, J & Bao, Z 2023, 'Salinity significantly affects methane oxidation and methanotrophic community in Inner Mongolia lake sediments', *Frontiers in Microbiology*, vol. Volume 13 - 2022, 2023-January-06.

Zhou, J, Theroux, SM, Bueno de Mesquita, CP, Hartman, WH, Tian, Y & Tringe, SG 2022, 'Microbial drivers of methane emissions from unrestored industrial salt ponds', *The ISME Journal*, vol. 16, no. 1, pp. 28

Appendices **:**

A: Metadata correlation matrix & water column profiles.

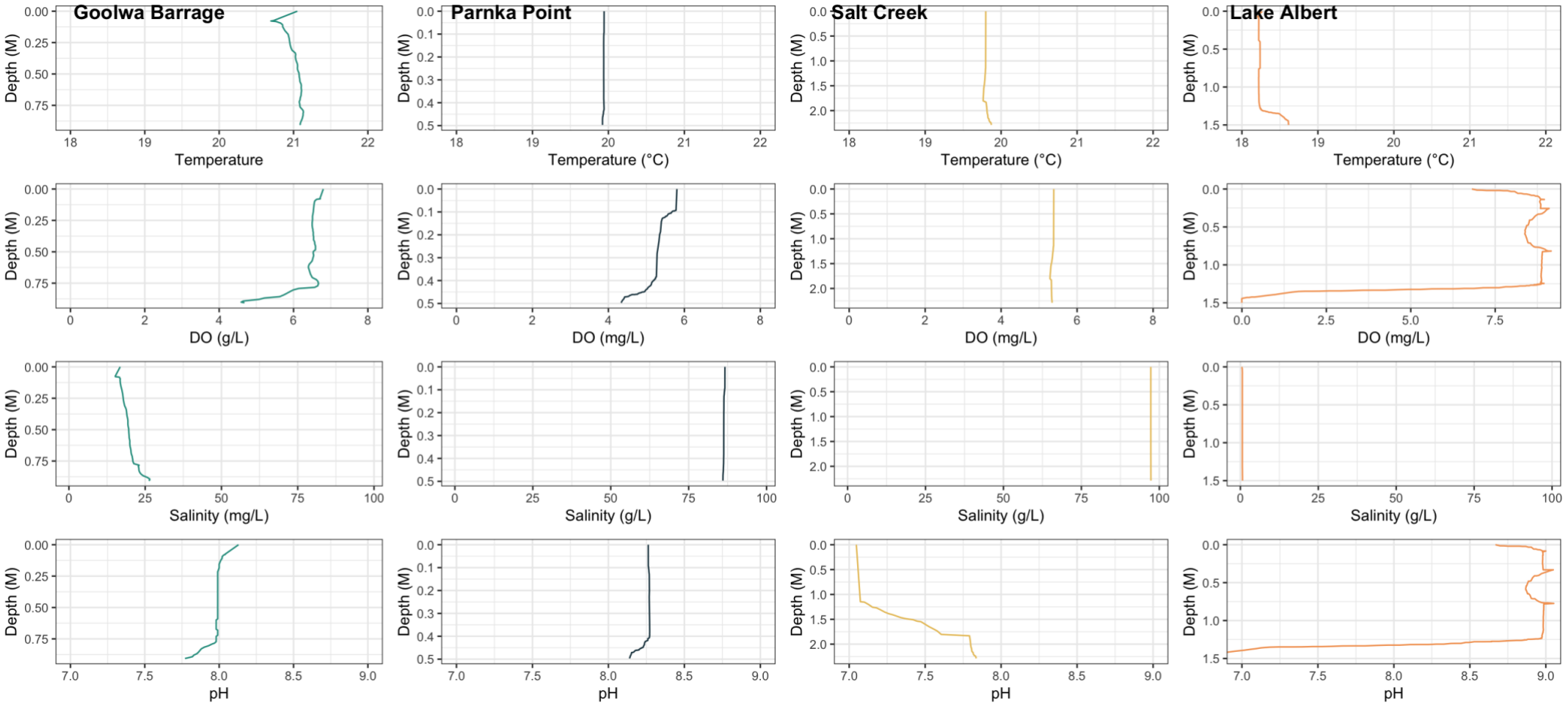

Figure A1: Water column profile for salinity, pH, temperature and dissolved oxygen for each site.

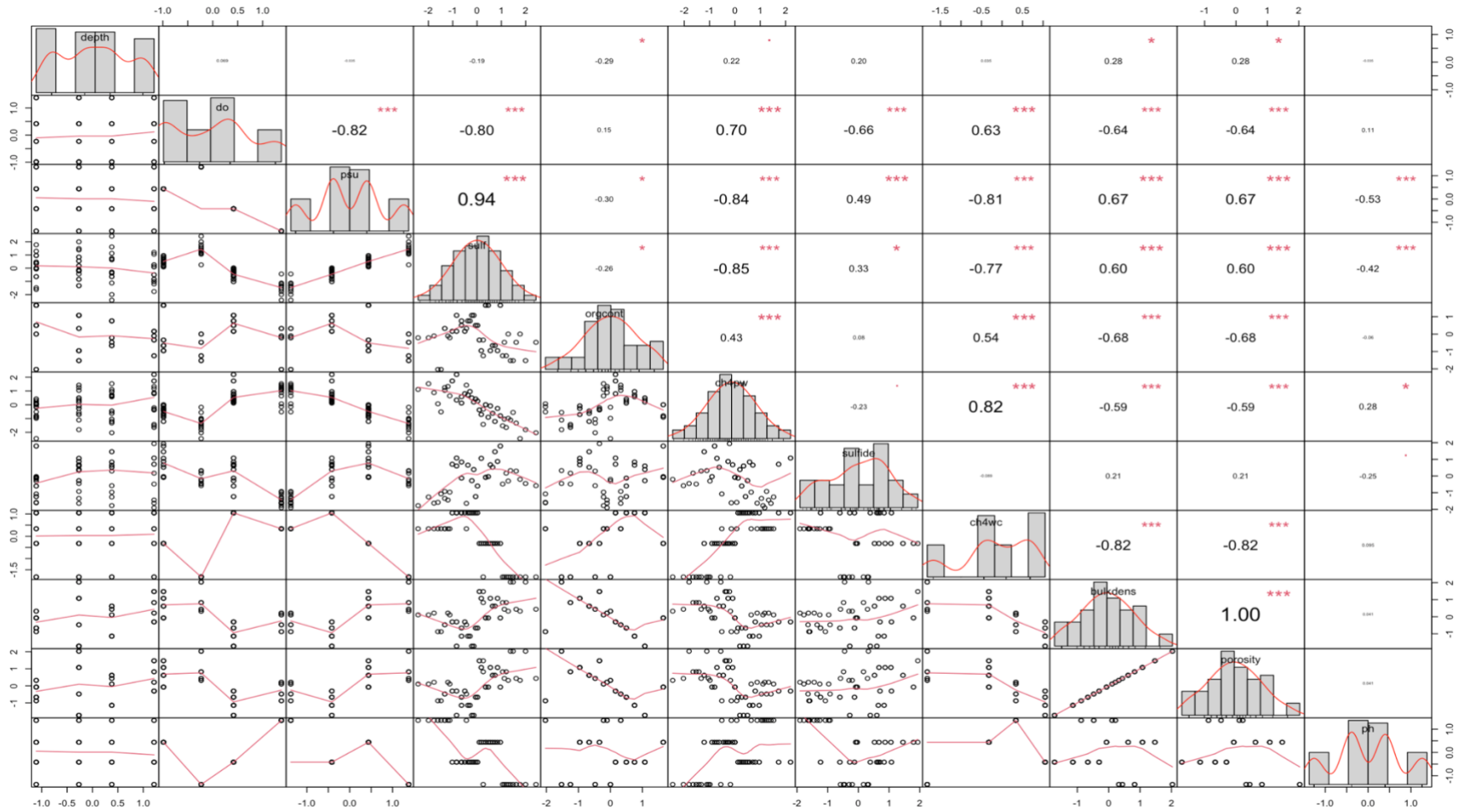

Figure A2: Correlation matrix of metadata variables as spearman's rank correlation coefficients. Significant correlations are denoted by the use of asterisks

B: Methane headspace equilibrium and saturation calculations

Methane headspace calculations

Porewater and water column dissolved methane was estimated using a headspace equilibration method. Methane headspace concentration is initially acquired in ppm derived from standard curves (**See Appendix F**). The initial concentration of methane in the site water samples (C_L^0) was related using methods in Johnson et al. (1990) for gases at equilibrium between gaseous and aqueous phases, outlined below:

$$C_L^0 V_L = C_L V_L + C_G V_G - C_{atm} V_G \qquad \textbf{Eq. 4}$$

where C_L^0 is the concentration of methane in the water before equilibration of interest (mol L^{-1}), C_L is the methane concentration in water after equilibrium, C_G is the methane concentration in the gas phase after equilibrium, and V_L and V_G are the volumes of liquid and gas phases, respectively. Subtracting the atmospheric methane concentration multiplied by headspace volume ($C_{atm}V_G$) accounts for background atmospheric methane concentrations in the headspace. The concentration of methane in the gas phase and water phase at equilibrium can be related by the partition coefficient K:

$$C_L = K \cdot C_G \qquad \textbf{Eq. 5}$$

Substituting **Eq. 5** into **Eq. 4**, gives **Eq. 6**.

$$C_L^0 = C_G(K + \frac{V_G}{V_L}) \qquad \textbf{Eq. 6}$$

Gas solubility is dependent on temperature, salinity, and pressure. To account for this, the partition coefficient was related to Henry's law constant (K_H) and the Bunsen solubility coefficient (β):

$$K_H = \frac{K}{RT} \quad \textbf{Eq. 7}$$

Where K_H is Henry's law constant, R is the ideal gas constant and T (K) is the air temperature. The Bunsen coefficient (β) can be then related to Henry's constant:

$$\beta = K_H(V_m) \quad \textbf{Eq. 8}$$

Where β is the Bunsen solubility coefficient (L L^{-1} atm^{-1}) and V_m is the molar volume of the gas (L mol^{-1}) adjusted for temperature. The Bunsen coefficient was calculated as per Wiesenburg and Guinasso (1979) (**See Eq. 23**).

Eq. 7 and **Eq. 8** allows the expansion of **Eq. 6**:

$$C_L^0 = C_G\left(\left(\frac{\beta}{V_m}\right)RT + \frac{V_G}{V_L}\right) \quad \textbf{Eq. 9}$$

The partial pressure of methane (p_{CH_4}) can be calculated using Dalton's Law of Partial Pressures:

$$p_{CH_4} = Px_{CH_4} \quad \textbf{Eq. 10}$$

Where p_{CH_4} is the partial pressure in the sample, P is the total pressure and x_{CH_4} is the mole fraction of methane in the sample. The mole fraction was directly derived from the gas chromatography output (ppm) and adjusted for water vapour presence using the relationship from Weiss (1980):

$$x_{CH_4} = x_{CH_4 unadjusted}\left(1 - \frac{p_{H_2O}}{P}\right) \quad \textbf{Eq. 11}$$

Where $x_{CH_4 unadjusted}$ is the mole fraction from the gas chromatography reading, and p_{H_2O} is the vapour pressure of water, calculated as a function of salinity and temperature as per Weiss (1980):

$$p_{H_2O} = e^{24.4543 - 67.4509\left(\frac{100}{T}\right) - 4.8489\left(\ln\left(\frac{T}{100}\right)\right) - 0.00054(S)} \quad \textbf{Eq. 12}$$

Where T is temperature (K), and S is salinity (%).

From the partial pressure, and using the ideal gas law, the concentration of methane in the headspace gas can be calculated:

$$\frac{n}{V} = \frac{p_{CH_4}}{RT} = C_G \quad \textbf{Eq. 13}$$

Where p_{CH_4} is the partial pressure of methane (atm). The concentration of methane in the headspace gas can then be related to the total methane concentration in the water sampling vessel.

$$C_L^0 = \left(\frac{p_{CH_4}}{RT}\right)\left(\left(\frac{\beta}{V_m}\right)RT + \frac{V_G}{V_L}\right) - C_{atm}V_G \quad \textbf{Eq. 14}$$

Methane Saturation Calculations

Methane saturation was calculated to understand the concentration of dissolved methane required to form bubbles within sediments, therefore facilitating ebullition. To calculate this, a modified version of Henry's Law was used as outlined in Schmid et al. (2004):

$$p_{CH_4} = H_{CH_4} \cdot [CH_4] \quad \textbf{Eq. 15}$$

Where p_{CH_4} is the partial pressure of CH_4, and $[CH_4]$ is the concentration of CH_4. Although, to account for *in-situ* temperature, salinity and pressure, an expanded relationship can be used:

$$f_{CH_4} = H_{CH_4}(T, S, P_0) \cdot [CH_4] \cdot e^{(P - P_0) \cdot V_{CH_4}/(R \cdot T)} \quad \textbf{Eq. 16}$$

$$p_{CH_4} = f_{CH_4} \cdot e^{-B_{CH_4}(T)\cdot P/(R\cdot T)} \quad \textbf{Eq. 17}$$

Where, f_{CH_4}represents the fugacity of CH_4, P is pressure, $P_0$is standard atmospheric pressure $V_{CH_4}$is the partial molal volume of dissolved CH_4, $B_{CH_4}(T)$ is the second virial coefficient for CH_4, R is the universal gas constant (Weiss 1974) and $H_{CH_4}$is Henry's Constant corrected for in-situ temperature, salinity and standard pressure. H_{CH_4} can be calculated and corrected for in-situ temperature as K_H from Sanders et al. (2021):

$$K_H = K_H^{\ominus} \times e^{\left(\frac{-\Delta_{soln}H}{R}\left(\frac{1}{T}-\frac{1}{T^{\ominus}}\right)\right)} \quad \textbf{Eq. 18}$$

Where, $K_H^{\ominus}$is henrys constant for CH_4 under standard conditions, $T^{\ominus}$is temperature at standard conditions and $-\Delta_{soln}H$ is the enthalpy of solution, which has the temperature dependence:

$$\frac{-d\ln k_H}{d(\frac{1}{T})} = \frac{-\Delta_{soln}H}{R} \quad \textbf{Eq. 19}$$

While this corrects for temperature, it doesn't factor in salinity, which can be done using the empirical Setschenow relation from Wilhelm et al. (1977):

$$\ln\gamma = k_S S \quad \textbf{Eq. 20}$$

Where $k_S S$ is the 'salting out' constant for methane corrected for in-situ salinity (ppt), and γ is the ratio of the solubility of a gas in pure water to that of seawater, $\gamma = {K_P}/{K_H}$, which can be rearranged to give:

$$K_H = \frac{K_P}{e^{k_S S}} \quad \textbf{Eq. 21}$$

The saturation concentration of methane can finally be calculated assuming that methane has a pure gas phase (**Eq. 15 & 16**).

C: Modelled methane fluxes

Atmospheric Diffusion Calculations

To compare to measured fluxes from chambers, diffusive methane fluxes from the water column to the atmosphere were calculated from surface water methane concentrations based on the methods outlined in Chaung et al. (2017), through using the gas transfer model of Wanninkhof (1992), and the general stagnant film equation (Liss and Slater 1974):

$$J = k_v \cdot (C_w - C_{eq}) \quad \textbf{Eq. 22}$$

Where J is flux of gas to the atmosphere (mmol m^{-2} d^{-1}), k_v is gas transfer velocity (m d^{-1}), C_w is measured water column methane concentration (mmol m^{-3}) and C_{eq} is concentration of methane in equilibrium with the atmosphere at in-situ temperature and salinity (mmol m^{-3}). C_{eq} was calculated for each sites temperature and salinity using the relationship developed in Wiesenburg and Guinasso (1979):

$$\ln C = A_1 + A_2\left(\frac{100}{T}\right) + A_3 \ln\left(\frac{T}{100}\right) + A_4\left(\frac{T}{100}\right) + S\%[B_1 + B_2\left(\frac{T}{100}\right) + B_3(\frac{T}{100})^2]$$

Eq. 23

Where C is equilibrium solubility (nmol/L), T is absolute temperature, $S\%$ is salinity (ppt) and A_{1-4} and B_{1-3} are constants. k_v was calculated using the gas transfer model of Wanninkhof (1992):

$$k_v = 0.31 \cdot u^2 \cdot (\frac{Sc}{660})^{-\frac{1}{2}} \quad \textbf{Eq. 24}$$

Where k_v is in cm h^{-1}, u is wind speed at 10m height (m s^{-1}), and Sc is the Schmidt number for methane derived from Jähne et al. (1987). Another approach is the model outlined by Tedford et al. (2014) which incorporates the importance of buoyancy flux β driven turbulence during cooling periods yielding the turbulent dissipation rate ε_{TE} as;

$$\varepsilon_{TE} = \begin{cases} \frac{C_1 U_{*w}^3}{KZ} + C_2|\beta| & if\ \beta < 0 \\ \frac{C_3 U_{*w}^3}{KZ} & if\ \beta > 0 \end{cases} \quad \textbf{Eq. 25}$$

Where c_1=0.56, c_2=0.77 and c_3=0.6 are dimensionless constants, u_{*w} is the friction velocity in the water, κ=0.41 is the von Kármán constant and depth z in which a constant 0.15 m was used. Friction velocity in the water u_{*w} was calculated from air friction velocity u_{*a}, which can be described using the drag coefficient C_d and the relationship outlined in Large & Pond (1981);

$$U_{*a} = U_{10} \cdot \sqrt{C_d} \quad \textbf{Eq. 26}$$

Friction velocity in the water u_{*w} can then be calculated as.

$$U_{*w} = U_{*a}\sqrt{\frac{p_a}{p_w}} \quad \textbf{Eq. 27}$$

Where p_a is air density and $p_w$is water density. Buoyancy flux can then be calculated according to Imberger (1985);

$$\beta = \frac{g a_t H_{eff}}{p_w C_p} \quad \textbf{Eq. 28}$$

Where g is gravitational accretion, $a_t$is coefficient of thermal expansion of water, H_{eff} is the effective heat flux (approximated as latent + sensible heat flux as per Friehe & Schmit (1976)), and C_p is the specific heat of water. Gas transfer velocity k can then be calculated according to the surface renewal model.

$$K_{TE} = C_4(\varepsilon_{TE} v)^{\frac{1}{4}} * Sc^{-\frac{1}{2}} \quad \textbf{Eq. 29}$$

where c_4=0.5 is a dimensionless constant and ν kinematic viscosity of water ($m^2\ s^{-1}$). K_{TE} can be subbed into **Eq. 22** resulting in the calculated diffusive flux.

Using U_{10} and water and air temperatures acquired from Water Data SA (DEW 2025) at hourly frequency, methane flux can be estimated using water column measurements from

each site over March (**figure S3**). It is key to note that various approximations were used in these calculations (effective heat flux & air friction velocity), which can be further restrained through paring sampling measurements with an anemometer.

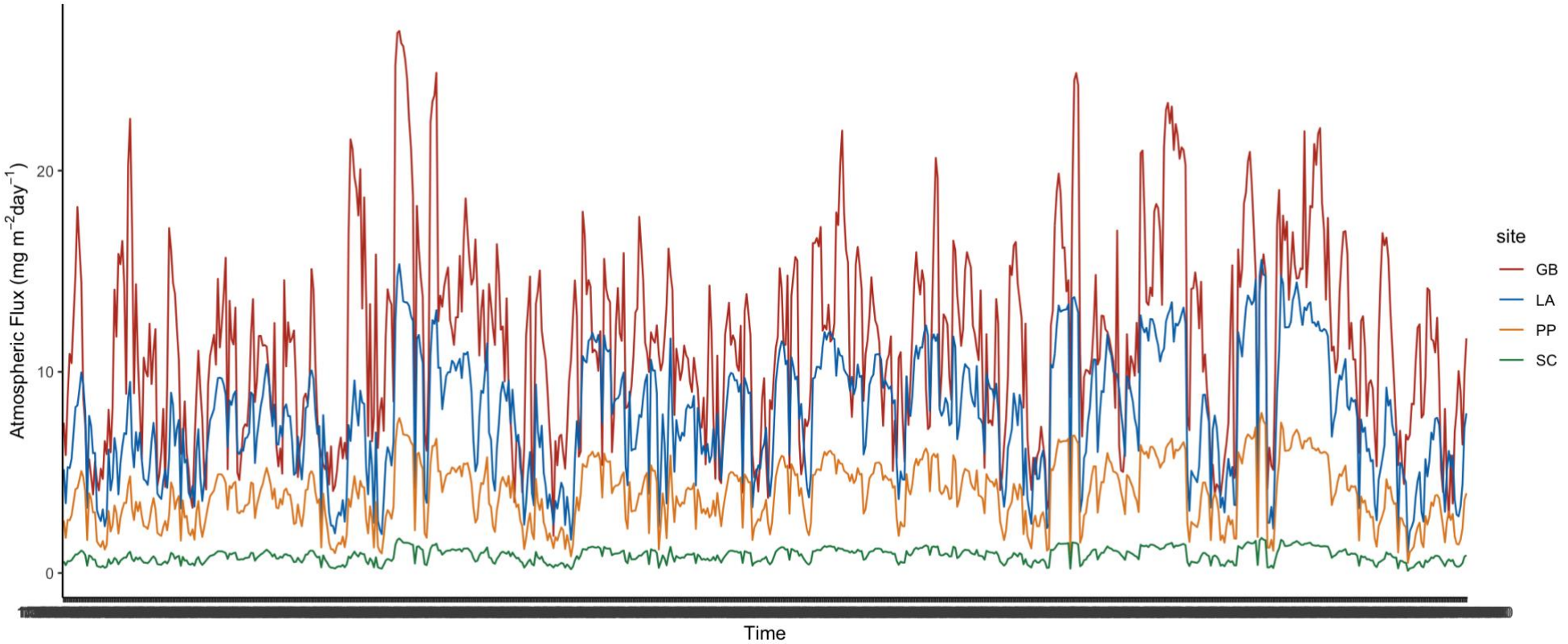

Figure A3: Hourly changes in calculated methane flux rates per site over the month of March. Data was acquired from the closet geographical point available on the Water Data SA database.

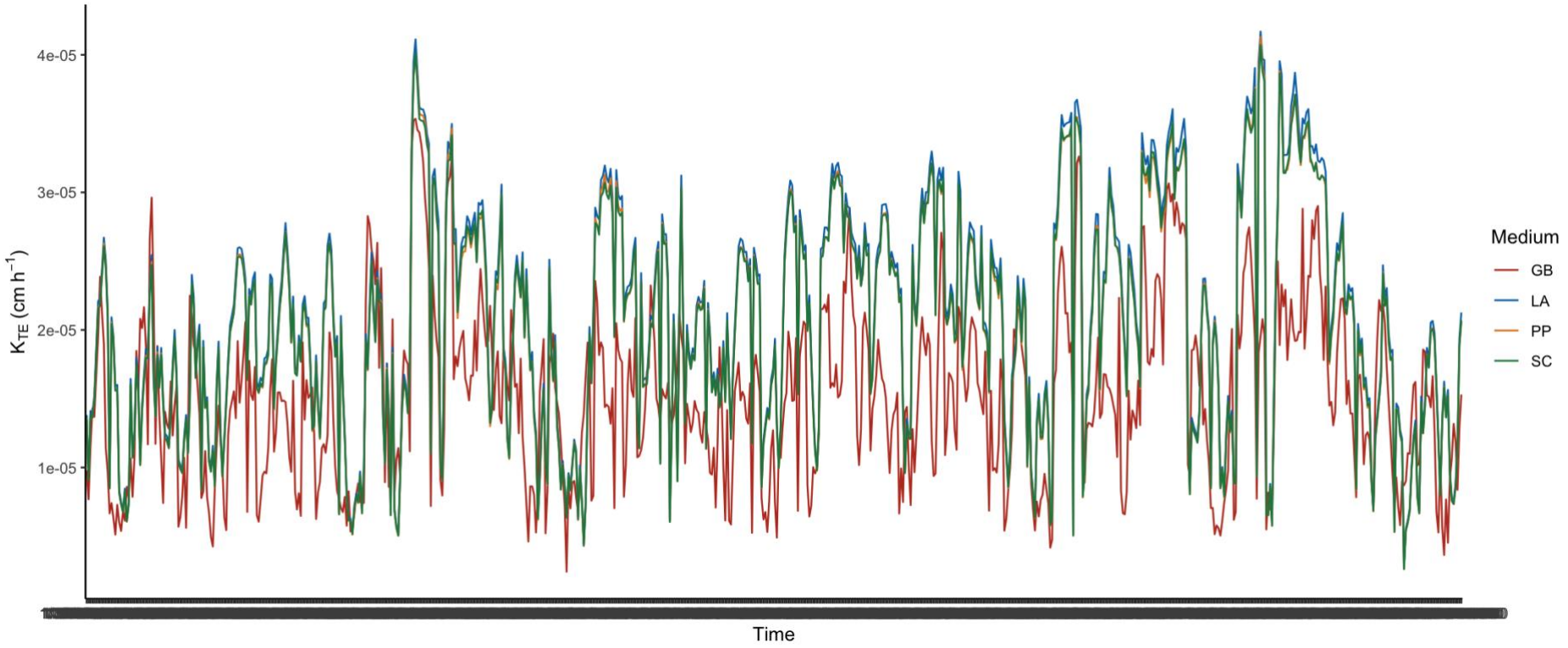

Figure A4: Hourly changes in K_{TE} per site over the month of March. Data was acquired from the closet geographical point available on the Water Data SA database.

D: FAPROTAX database adjustments.

Due to the conservatism of the FAPROTAX approach (e.g. reliance on cultured strains of notoriously difficult-to-culture Archaea from extreme environments) (Solden et al. 2016), slight modifications were applied to broaden the scope of the database. These mainly included using family level classifications as well as some manual adjustments to the database to include various methylotrophic methanogens classifications where either a) no cultured strains exist, but the function is well supported by genomic approaches in the literature; or b) where function has been verified in pure culture, but it is not yet represented in the FAPROTAX database. General adjustments to the FAPROTAX pipeline (applying the database) are outlined in **Table A1**, and database specific substitutions are outlined in **Table A2.** The large proportion of "not described" pathways in hypersaline is predominantly due to shallow classification of methylotrophic methanogens from the order "*Methanofastidiosales*" which did not meet the family level classification set. An original distribution of methanogen pathways before database edits can be seen in **Figure A5.**

Table A1: General Adjustments made to the FAPROTAX pipeline.

Adjustment	**Justification**
Pipeline to detect taxonomy from family level.	Taxonomic classification can be challenging in extreme environments. Therefore, the pipeline was adjusted to infer function based on taxonomy at the Family level rather than the Genus level.
Pipeline adjustment to detect species level identifications with "uncultured_" as a prefix	The FAPROTAX pipeline removes any OTUs that have 'uncultured' within taxonomy labels. As a result OTUs classified at genus or family level, but have 'uncultured' labelled at species level are removed. This adjustment allows for several Genera in the dataset.

Table A2: Manual adjustments to FAPROTAX database with justification provided.

Action	Justification	Reference
Methyloceanibacter to 'Methanotrophy" & "Methylotrophy"	Validated ability to oxidise methanol & methane in all cultured species. Hence all members of the Genus are highly likely to be involved in methane consumption.	Takeuchi et al. 2014; Vekeman et al. 2016.
Methermicoccus & *Methermicoccaceae* to "methylotrophic methanogenesis"	Methylotrophic methanogenesis using substrates methanol & methylamine substrates is validated in pure culture across both Family and Genus levels.	Cheng et al. 2007
Methanonatronarchaeum to "methylotrophic methanogenesis"	Extremely halo(natrono)philic methyl-reducing methanogenesis is validated in pure and mixed culture across this phylogenetic lineage.	Sorokin et al. 2018
Methanocella to "hydrogenotrophic methanogenesis"	Hydrogenotrophic methanogenesis is validated in all pure cultures across the Genus.	Sakai et al. 2008
"Methanofastidiosum" to "methylotrophic methanogenesis"	This Genus of Archaea has been identified through thorough deep metagenomic analysis and MAG construction. While it is notoriously difficult to obtain pure cultures of this organism, there is strong genomic evidence to support *Methanofastidiosum* harbours the genes required for methylotrophic methanogenesis. There is further evidence to suggest these taxa are highly correlated to methane production in the Coorong's South Lagoon.	Nobu et al. 2016 Keneally et al. 2024
"Methanomethylicus" to "methylotrophic methanogenesis"	All members of this Genus of Archaea remain uncultured, but strong genomic evidence and MAG reconstruction has led to well supported inference of their ability to perform methanogenesis by methylated thiol reduction.	Vanwonterghem et al. 2016

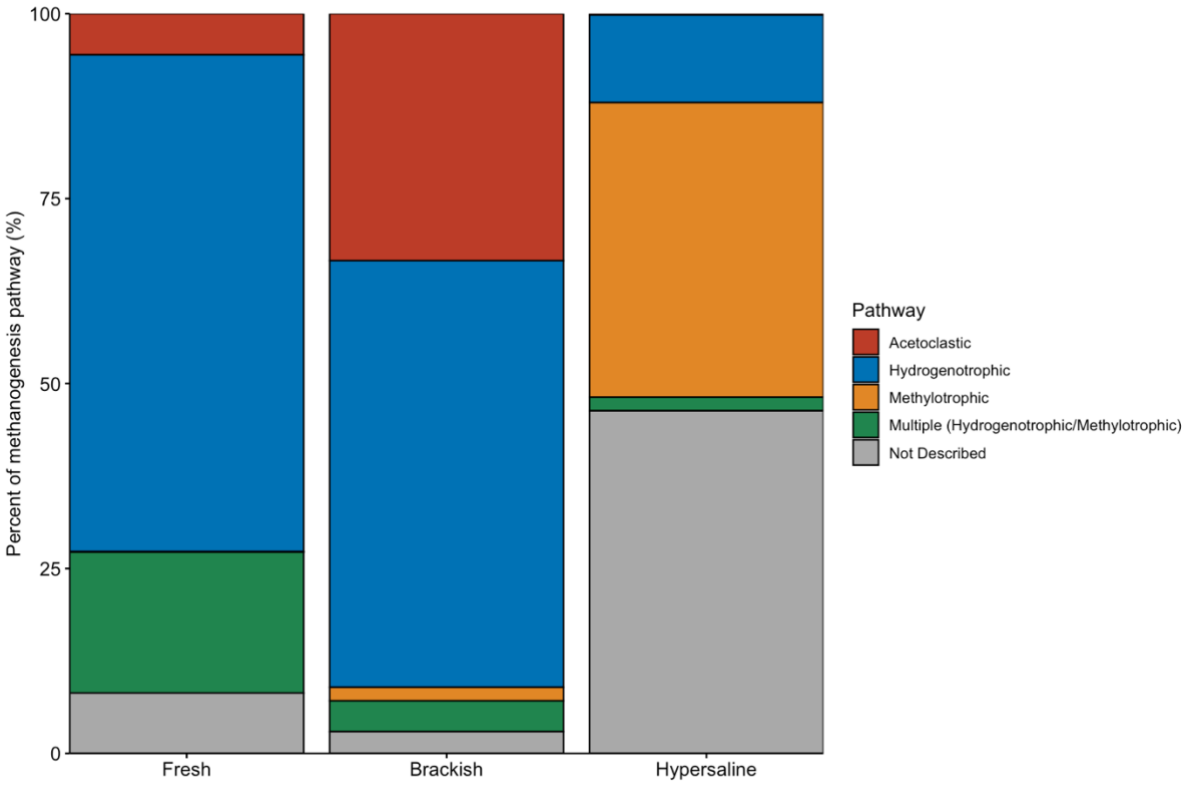

Figure A5: Proportion of methanogenesis pathways occurring at each salinity group before Manual database adjustments (table A2). Methanogenesis pathways were identified based on the relative proportion of methanogenic OTUs associated with each pathway as determined by FAPROTAX.

E: Microbial community functional gene and pathway inference for hypothesis generation

To predict community metabolism Kyoto Encyclopedia of Genes and Genomes (KEGG) orthologs were predicted from ASVs using PICRUSt2 (Douglas et al. 2020). As 16s-based gene predictions are inferred from known sequenced and reference genomes, the generated data of this method should be interpreted with care. Predicted activity from 16S does not confirm metabolic activity during sampling or does not prove the presence of specific genes. To minimise potentially errors, proper quality control should be put into place. To reduce noise ASVs observed less than 3 times and not observed within two samples were removed from the data. KEGG orthologs were mapped to pathways with *ggpicrust2* (Yang et al. 2023). Differential abundance testing on pathways, and specific orthologs of interest was performed with *DESeq2*'s Wald test (Love et al. 2014).

Predicted gene expression profiles generated using PICRUSt2 revealed significant differences across the salinity gradient. Genes encoding all three subunits (*mcrA, mcrB*, and *mcrG*) of methyl-coenzyme M reductase, the enzyme catalysing the final step of methanogenesis, were enriched in fresh and brackish samples compared to hypersaline sites (**Figure A6**). Conversely, predicted genes encoding coenzyme M methyltransferases (*mttC*, *mttB*, and *mtmB*) were enriched in hypersaline samples. Key genes associated with the hydrogenotrophic methanogenesis pathway (*mtrB*, *mtrC*, *mtrD, mtrE, mtrF,* and *mtrG*) were significantly enriched in fresh and brackish sediments. In contrast, genes related to the acetoclastic pathway showed slight enrichment in hypersaline samples, likely reflecting the use of these genes in general carbon cycling processes (e.g., the acetyl-CoA pathway).

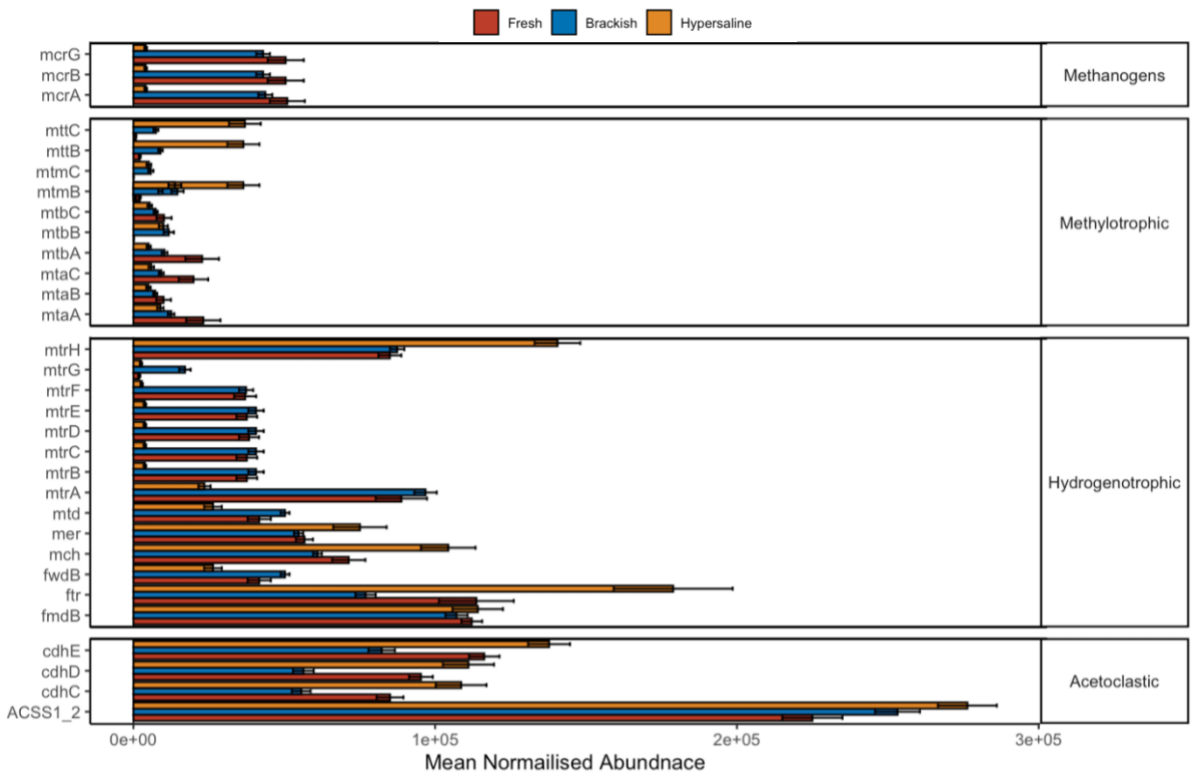

Figure A6 : Normalised abundance of predicted genes. KEGG orthologs of interest are categorized by relevant methanogenic metabolic pathway (right labels) and visualized corresponding normalised abundance. Salinity groups are visualised as different colours.

Predicted genes coding for MCR (*mcrA/B/G*) were significantly enriched within fresh and brackish sites indicating that overall, methanogenesis was likely occurring at a lower rate at hypersaline sites. Genes related to methylotrophic methanogenesis, coding for trimethylamine transferase (*mttB/mttC*) and Co-methyltransferase (*mtmB*) were all enriched within hypersaline sites, while key hydrogenotrophic genes such as *mtrA/B/C/D/E/F/G* coding for the Mtr complex were enriched within brackish and fresh sites. Hypersaline sites were also enriched in acetyl-CoA synthetase (*acs*) and acetyl-CoA decarbonylase (*cdhC/D/E*) encoding genes. Although, Acetyl-CoA is essential for many organisms and utilised more broadly in central carbon metabolism indicating the

presence of intense competition for these resources (Starai and Escalante-Semerena 2004).

It is key to note that these results are intended as predictive, where this approach has generated useful hypotheses in analogous environments (Menéndez-Serra et al. 2019). To validate these predictions future metabolite-based experimental functional analyses should be performed, focused on clarifying the availability, transport, and degradation of methylated compounds (Keneally et al. 2024).

F: Gas Chromatography Method Development

To measure methane concentration from gas headspace sampling, a processing method was developed using a gas chromatography flame ionisation detector (GC-FID) with the aid of Dr Tony Hall. The method had the following aims:

To effectively process samples for methane concentration using an Agilent 7890B GC-FID system, a set of objectives were designed to achieve through method development. These objectives include:

1. The GC method must have high resolution and therefore peak separation for CH_4.
2. The GC method must have a high sensitivity and signal to noise ratio (SNR) to detect low concentrations of CH_4.
3. The GC method must have high throughput to process large numbers of samples efficiently.
4. The GC method must be compatible for 'dirty' environmental samples
5. The GC method must provide qualitative assessment of CH_4 (Identification).

This will allow for fine-tuning of the GC-FID system to effectively process CH_4 samples from a range of sources. Outlined below is some of the chromatographs and calibration curves developed during processing.

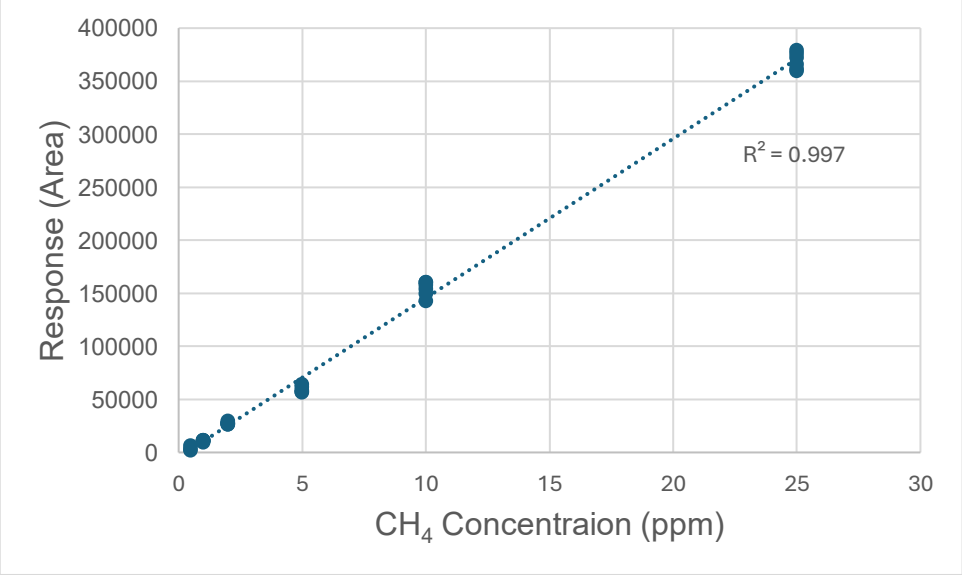

Figure A5: Calibration curve of CH_4 in N_2 from 25-0.5ppm. The R^2 value is 0.997.

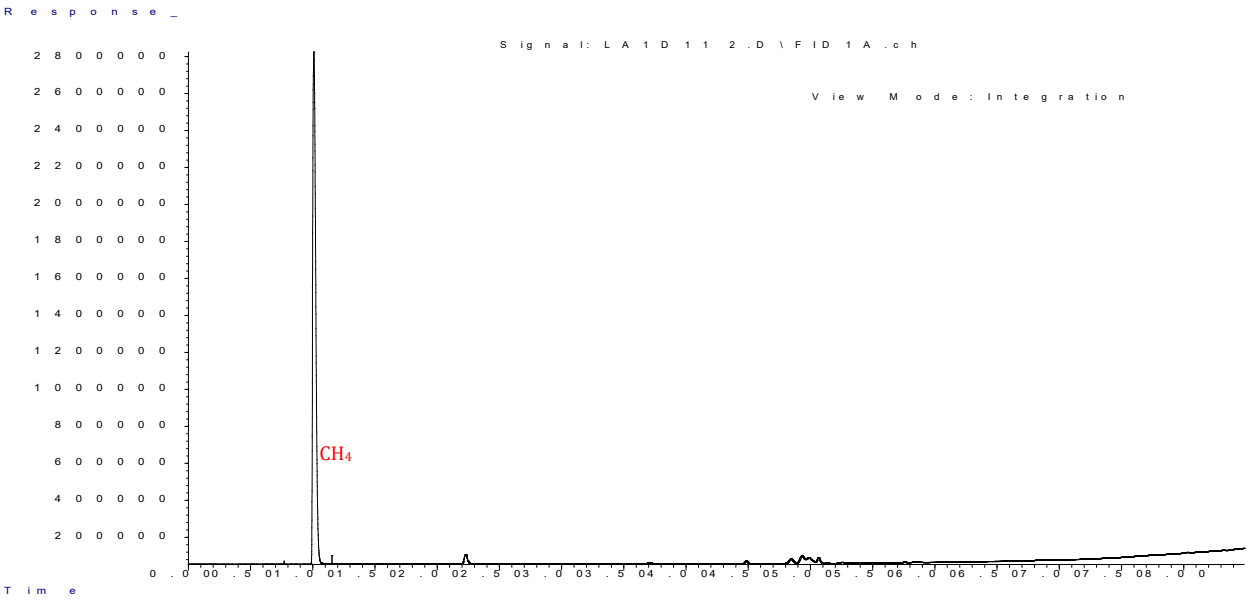

Figure A6: Chromatograph of high concentration porewater sample from the site 'GB'. The injection volume was 500µL.

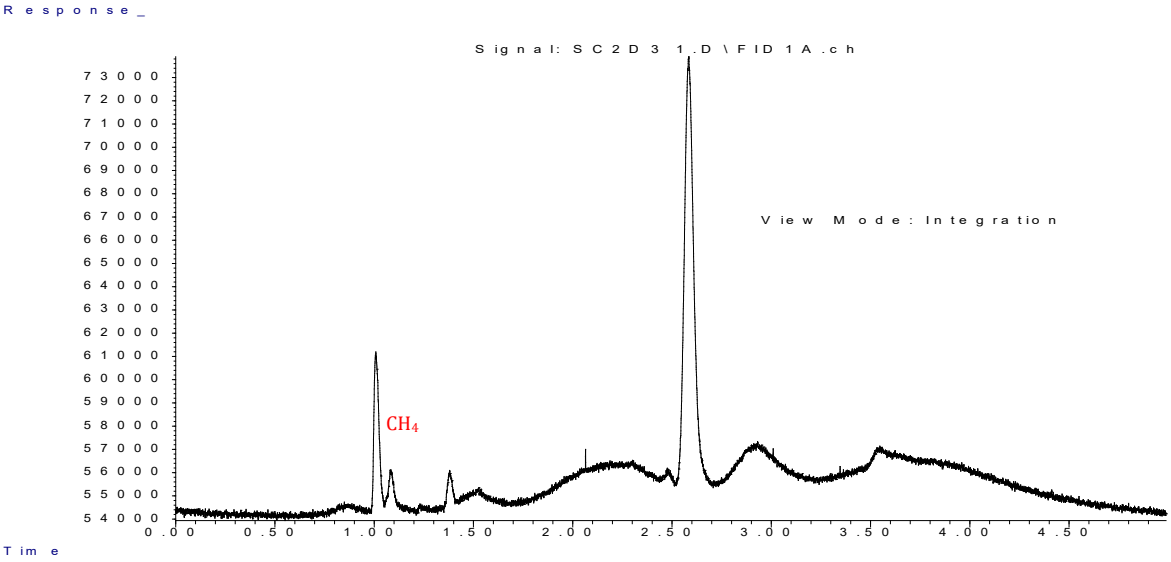

Figure A7: Chromatograph of low concentration porewater sample from the site 'SC. The injection volume was 500µL.

G: Sulfide DGT processing

Sulfide DGT probes can measure *in situ* 2D representations of analyte concentrations. Examples of these representations can be seen below.

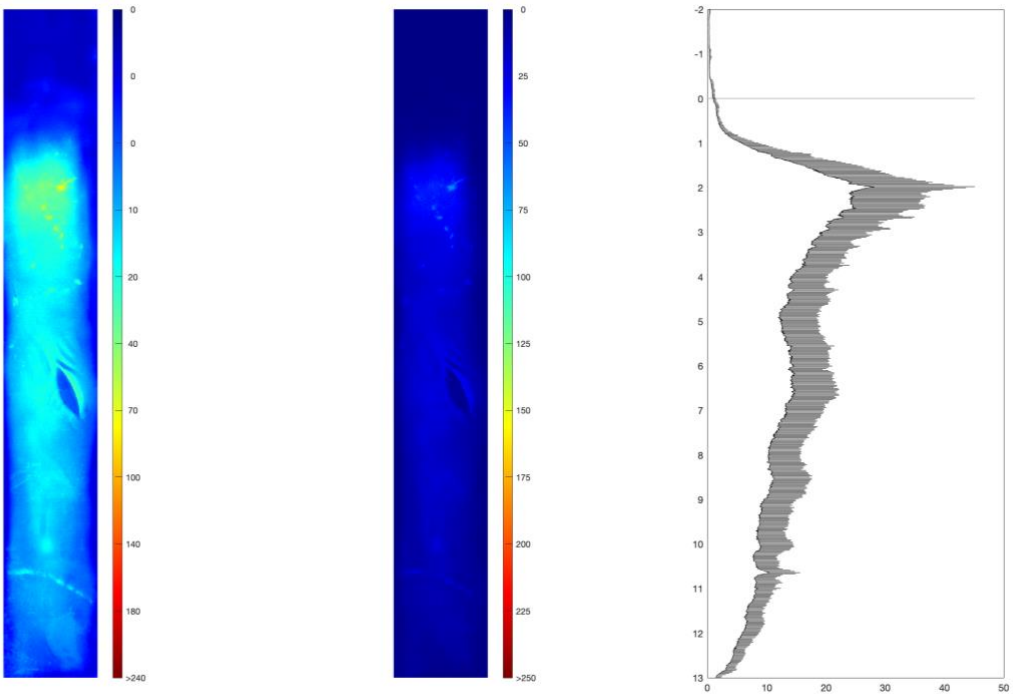

Figure A8: Heatmap representation of sulfide concentrations where A) total sulfide accumulated, B) calculated concentration of sulfide and C) concentration over sediment depth. Note that ellipse within A & B refer to tears due to coarse sediment when sampling and was accounted for when processing. This sample is from Lake Albert.

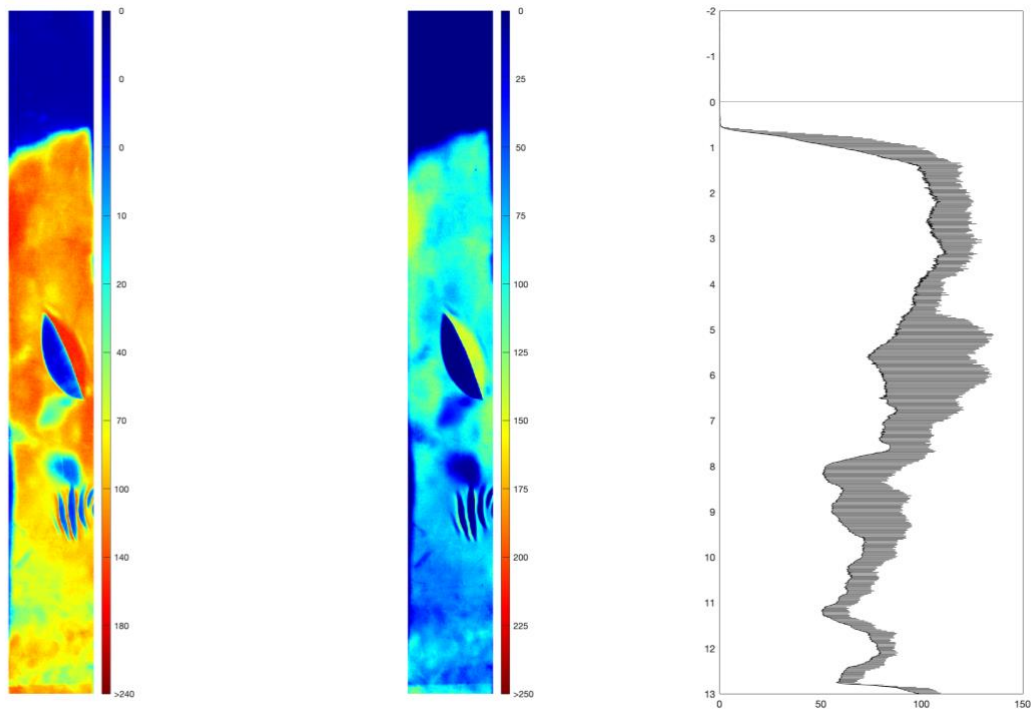

Figure A9: Heatmap representation of sulfide concentrations where A) total sulfide accumulated, B) calculated concentration of sulfide and C) concentration over sediment depth. Note that ellipse within A & B refer to tears due to coarse sediment when sampling and was accounted for when processing. This sample is from Salt Creek.

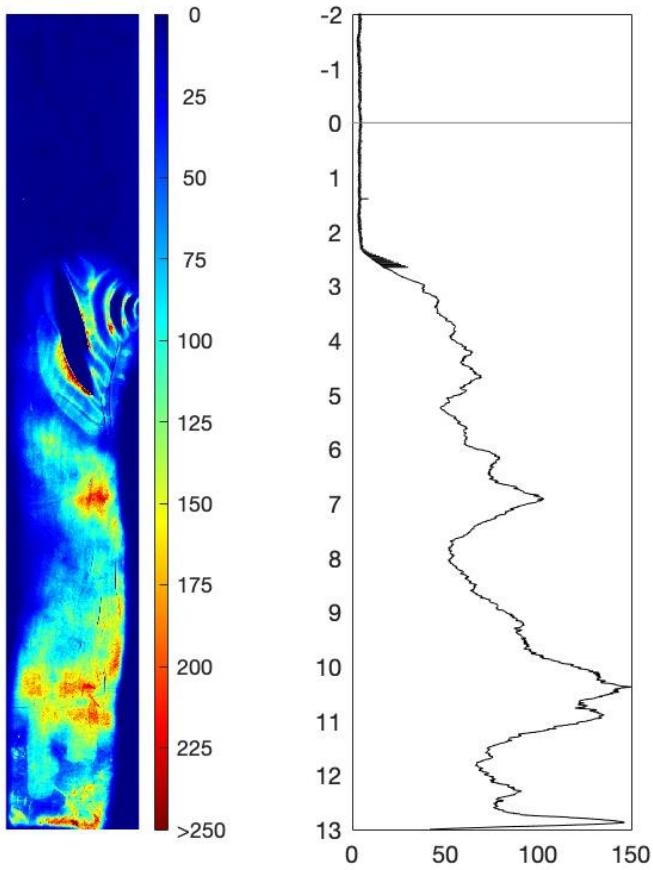

Figure A9: Heatmap representation of sulfide concentrations where A) total sulfide accumulated, B) calculated concentration of sulfide and C) concentration over sediment depth. Note that ellipse within A & B refer to tears due to coarse sediment when sampling and was accounted for when processing. This sample is from Parnka Point.

Figure A10: Setup for sulfide DGT processing. Deployed DGT probes can be seen on the left with site water being circulated over them.